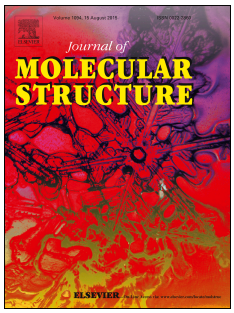

Synthesis, X-ray structure, vibrational spectroscopy, DFT, biological evaluation and molecular docking studies of (*E*)-*N'*-(4-(dimethylamino)benzylidene)-5-methyl-*1H*-pyrazole-3-carbohydrazide

Khalid Karrouchi, Silvia A. Brandán, Yusuf Sert, Hakima El-marzouqi, Smaail Radi, Marilena Ferbinteanu, My El Abbes Faouzi, Yann Garcia, M'hammed Ansar

PII: S0022-2860(20)30866-8

DOI: https://doi.org/10.1016/j.molstruc.2020.128541

Reference: MOLSTR 128541

To appear in: *Journal of Molecular Structure*

Received Date: 17 April 2020

Revised Date: 15 May 2020

Accepted Date: 26 May 2020

Please cite this article as: K. Karrouchi, S.A. Brandán, Y. Sert, H. El-marzouqi, S. Radi, M. Ferbinteanu, M.E.A. Faouzi, Y. Garcia, M'. Ansar, Synthesis, X-ray structure, vibrational spectroscopy, DFT, biological evaluation and molecular docking studies of (*E*)-*N'*-(4-(dimethylamino)benzylidene)-5-methyl-*1H*-pyrazole-3-carbohydrazide, *Journal of Molecular Structure* (2020), doi: https://doi.org/10.1016/j.molstruc.2020.128541.

Author statement

Khalid Karrouchi: Conceptualization, Methodology, Original Draft, Writing - Review & Editing.

Silvia A. Brandán : Theoretical, Calculations Writing - Original Draft, Writing - Review & Editing.

Yusuf Sert: Theoretical, Calculations Writing - Original Draft.

Hakima El-marzouqi: Resources.

Smaail Radi: Supervision, Project administration.

Marilena Ferbinteanu: Software, Validation, Writing - Review.

My El Abbes Faouzi : Visualization, Investigation.

Yann Garcia: Supervision, Investigation

M'hammed Ansar: Supervision, Project administration.

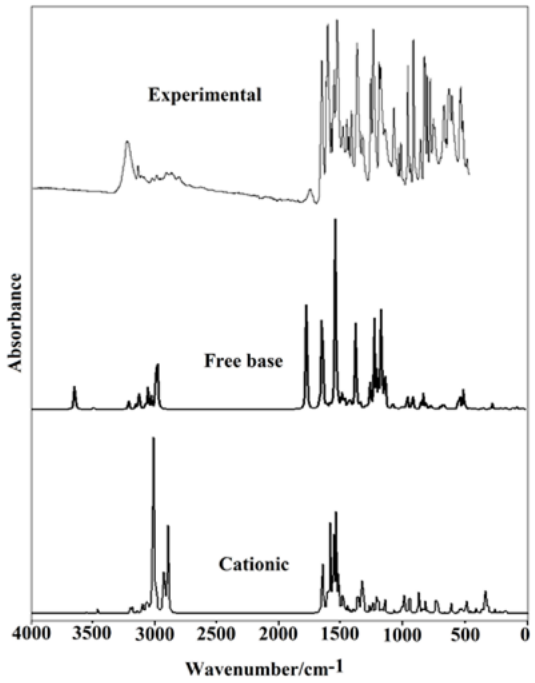
Experimental
Free base
Cationic
Absorbance
4000 3500 3000 2500 2000 1500 1000 500 0
Wavenumber/cm-1

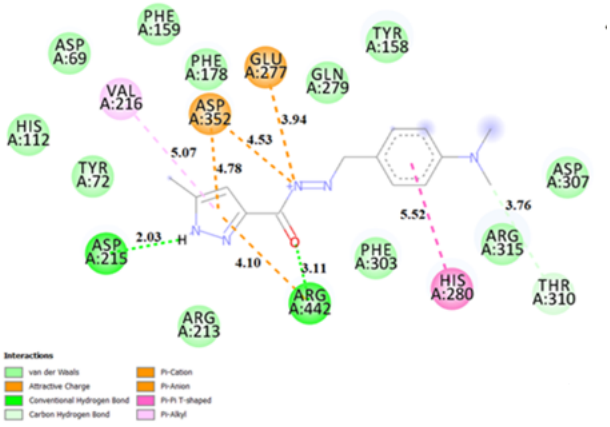
PHE A:159
ASP A:69
PHE A:178
GLU A:277
TYR A:158
GLN A:279
VAL A:216
ASP A:352
HIS A:112
TYR A:72
ASP A:307
ASP A:215
PHE A:303
ARG A:315
HIS A:280
THR A:310
ARG A:442
ARG A:213
3.94
4.53
5.07
4.78
2.03
4.10
3.11
5.52
3.76
Interactions
van der Waals
Attractive Charge
Conventional Hydrogen Bond
Carbon Hydrogen Bond
Pi-Cation
Pi-Anion
Pi-Pi T-shaped
Pi-Alkyl

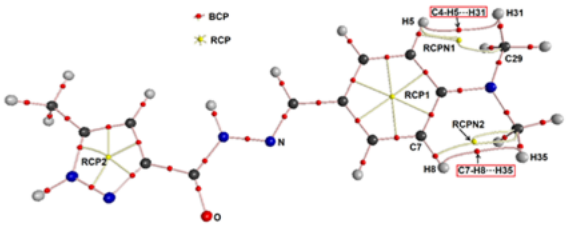
BCP
RCP
C4-H5···H31
H5
H31
RCPN1
C29
RCP1
RCPN2
C7
H8
H35
C7-H8···H35
RCP2
N
O

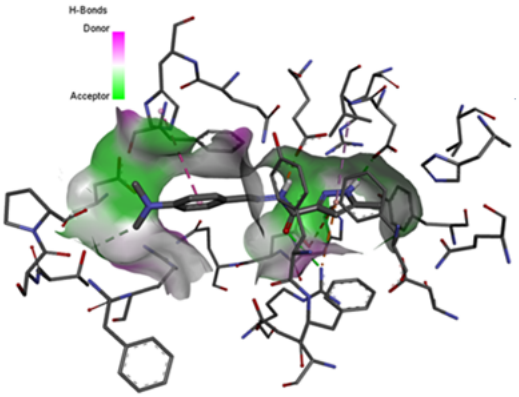
H-Bonds
Donor
Acceptor

Synthesis, X-ray structure, Vibrational spectroscopy, DFT, biological evaluation and molecular docking studies of (*E*)-*N'*-(4-(dimethylamino)benzylidene)-5-methyl-*1H*-pyrazole-3-carbohydrazide

Khalid Karrouchi [a,*], Silvia A. Brandán [b,*], Yusuf Sert [c], Hakima El-marzouqi [d], Smaail Radi [e], Marilena Ferbinteanu [f], My El Abbes Faouzi [d], Yann Garcia [g], M'hammed Ansar [h]

[a] *Laboratory of Analytical Chemistry and Bromatology, Faculty of Medicine and Pharmacy, Mohamed V University, Rabat, Morocco.*

[b] *Cátedra de Química General, Instituto de Química Inorgánica, Facultad de Bioquímica, Química y Farmacia, Universidad Nacional de Tucumán, Ayacucho 471, 4000, Tucumán, Argentina.*

[c] *Sorgun Vocational School, Science and Art Faculty-Department of Physics, Yozgat Bozok University, Yozgat, Turkey.*

[d] *Laboratory of Pharmacology and Toxicology, Pharmacokinetic Research Team, Faculty of Medicine and Pharmacy, University Mohammed V, Rabat, Morocco*

[e] *Laboratory of Applied Chemistry and Environment (LCAE), Department of Chemistry, Faculty of Sciences, University Mohamed Premier, Oujda 60000, Morocco.*

[f] *Inorganic Chemistry Department, Faculty of Chemistry, University of Bucharest, Dumbrava Rosie 23, Bucharest 020462, Romania.*

[g] *Institute of Condensed Matter and Nanosciences, Molecular Chemistry, Materials and Catalysis (IMCN/MOST), Université catholique de Louvain, Place L. Pasteur 1, 1348 Louvain-la-Neuve, Belgium.*

[h] *Laboratory of Medicinal Chemistry, Faculty of Medicine and Pharmacy, Mohamed V University, Rabat, Morocco.*

*****Corresponding authors:

Khalid.karrouchi@um5s.net.ma (K. Karrouchi)

brandansa@yahoo.com.ar (Silvia A. Brandán)

Abstract

New crystal, (*E*)-*N'*-(4-(dimethylamino)benzylidene)-5-methyl-*1H*-pyrazole-3-carbohydrazide (**3**) has been synthesized and characterized by FT-IR, NMR, ESI-MS and single crystal X-ray diffraction (XRD). The optimized molecular structures of free base and cationic species of (**3**) in gas phase and aqueous solution, vibrational frequencies and, corresponding vibrational assignments have been investigated experimentally and theoretically by using the B3LYP/6-31G* and B3LYP/6-311++G** methods. High solvation energy values are observed for both species of (**3**) in solution while the NBO and AIM studies support the higher stability of the cationic species in solution. The high energy values $\Delta E_{\sigma\rightarrow\sigma^*}$ and $\Delta E_{\sigma\rightarrow\pi^*}$ transitions, due to the planarity of both CH_3 groups linked to N atom, could support the high reactivities of its free base and cationic species, as compared with naloxone, cocaine and scopolamine. Complete vibrational assignments of 105 and 108 vibration modes expected for free base and cationic species of (**3**) together with the corresponding harmonic force constants are here reported. *In vitro* antidiabetic and antioxidant activities were revealed for (**3**). The molecular docking studies of the title compound revealed that it may exhibit anti-diabetic activity via inhibition of α-glucosidase PDB:3A4A enzyme.

Keywords: Pyrazole; Crystal structure; Vibrational spectroscopy; DFT; NBO; Antioxidant activity; Antidiabetic activity; Molecular docking.

1. Introduction

Hydrazones, carbohydrazides and similar derivatives represent an important class of organic compounds of interest in the medicinal and pharmaceutical fields [1-11] because one of many studies has reported that hydrazones improve the antitumor selectivity and toxicity profile of antitumor agents by forming drug carrier systems employing suitable carrier proteins [5]. Other studies have evidenced that many pyrazole derivatives present therapeutic activity [12-17], some are pesticides [18-20] and, other exhibit a wide gamma of biological properties, such as anti-inflammatory, anti-cancer, antioxidants, antidepressants, antivirals, analgesics, anti-parkinsons, anti-alzheimer, anti-glaucoma, anti-diabetic, anti-tubercular and anti-leishmanial [21-35]. With this background set, the determinations of structural, electronic and topological properties of these pyrazole derivatives are essential to know the influence of different groups on the structures in order to understand the connections of these groups with their biological properties. On the other hand, the vibrational analyses and, in particular the vibrational assignments of all bands observed in the experimental infrared and Raman spectra are of great aid to identify all species in any medium, especially when these studies are combined with theoretical calculations derived from density functional theory (DFT) [36-39].
In the present work, a new crystalline derivative has been synthesized, (*E*)-*N'*-(4-(dimethylamino)benzylidene)-5-methyl-*1H*-pyrazole-3-carbohydrazide (**3**) and, then it was characterized by using FT-IR spectrum in the solid phase, ^{1}H- and ^{13}C-NMR spectra in DMSO-d_6 solution, ESI-MS and single crystal X-ray diffraction (XRD). These experimental studies were accomplished with theoretical DFT calculations by using the functional hybrid B3LYP together with the 6-311++G** basis set in order to predict the structural, electronic, topological and vibrational properties in the gas phase [40,41]. Taking into account the wide range of biological activities reported for pyrazole derivatives, this new derivative was here evaluated by *in vitro* anti-diabetic and anti-oxidant activities. Hence, the reactivities of this derivative in gas phase and in aqueous solution were predicted by using the frontier orbitals with the B3LYP/6-311++G** method while their behaviours in both media were evaluated calculating some descriptors useful for compound containing different type of rings [42-51]. All calculations in aqueous solution were performed with the self-consistent reaction field (SCRF) method by using the integral equation formalism variant polarised continuum (IEFPCM) and universal solvation models [52-54]. The bands observed in the experimental infrared spectrum were assigned by using the harmonic force field calculated with the SQMFF methodology and the Molvib program at the same level of theory [55-57]. Here, the

main scaled force constants by using the same level of theory were reported for this new pyrazole derivative. Comparisons among experimental and predicted FT-IR, ^{1}H- and ^{13}C-NMR spectra have showed reasonable concordance among them. In addition, the interactions of the title molecule with α-Glucosidase PDB:3A4A and antioxidant peroxiredoxin 5 PDB:1HD2 receptors were investigated by molecular docking studies.

2. Experimental section

2.1. General methods

All chemical reactions were purchased Sigma-Aldrich. Reactions were checked with TLC using aluminum sheets with silica gel 60 F254 from Merck. Melting points were measured using a Buchi B-545 digital capillary melting point apparatus and used without correction. The FT-IR spectrum was recorded with Perkin-Elmer VERTEX 70 FT-IR spectrometer covering field 400–4.000 cm^{-1}. ^{1}H and ^{13}C NMR spectra were recorded in solution in DMSO-d_6, on Bruker spectrometer (300 MHz). The chemical shifts are expressed in parts per million (ppm) by using tetramethylsilane (TMS) as internal reference. Mass spectra were collected using API 3200 LC/MS/MS system, equipped with an ESI source.

2.2. Synthesis

General procedure for the synthesis of (E)-N'-(4-(dimethylamino)benzylidene)-5-methyl-1H-pyrazole-3-carbohydrazide (**3**) :

Target compound (**3)** described here was facilely synthesized according to the literature procedures [58-61] (Scheme 1). To a solution of 5-methyl-*1H*-pyrazole-3-carbohydrazide (**1**) (1 mmol) in 10 mL of ethanol was added an equimolar amount of the 4-dimethylaminobenzaldehyde (**2**) in the presence of two drops of acetic acid. The mixture was maintained under reflux for 2 h, until TLC indicated the end of reaction. Then, the reaction mixture was poured in cold water, and the precipitate formed was filtered out washed with ethanol and recrystallized from ethanol.

Yield 81 %, M.p. 259-261 °C; IR (ATR, ν(cm^{-1})) : 3233 (NH), 1648 (C=O), 1602 (N=CH); ^{1}H-NMR (300 MHz, DMSO-d_6, δ(ppm)): δ = 2.26 (s, 3H, CH_3), 2.94 (s, 6H, $N(CH_3)_2$), 6.45 (s, 1H, H-pyrazole), 6.72 (d, J = 8.7 Hz, 2H, H-Ar), 7.46 (d, J = 8.7 Hz, 2H, H-Ar), 8.30 (s, 1H, -NH), 11.24 (s, 1H, N=CH) 13.01 (s, 1H, NH-pyrazole) ; ^{13}C NMR: (300MHz, DMSO-d_6, δ (ppm)): 10.78, 40.28, 105.11, 112.26, 122.33, 128.76, 140.36, 146.60, 148.42, 151.84, 158.45. MS: m/z = 272.3 $(M+H)^{+}$.

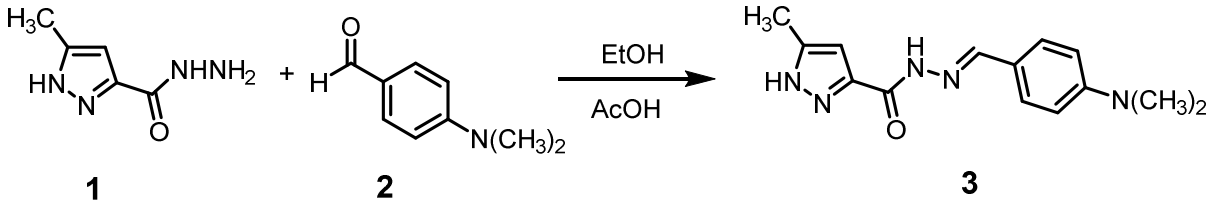

1 2 3

Scheme 1. The synthetic route of compound **3**.

2.3. Single crystal X-ray diffraction

X-ray single crystal data were collected by using MoKα (λ = 0.71075 Å) radiation on a Rigaku R-Axis Rapid II diffractometer equipped with an large-area curved imaging plate detector (460.0 x 256.0 mm), 3-circle goniometer and high-frequency 5 kW sealed tube. All calculations were performed using the CrystalStructure [62] crystallographic software package except for refinement, which was performed using the software package Olex1.2 [63]. The structure was solved by direct methods and refined in a routine manner (SHELXL) [64]. Non-hydrogen atoms were refined anisotropically. Hydrogen atoms were refined using the riding model. Molecular graphics were generated by using MERCURY 3.9 [65] and POV-Ray software [66]. The details of the X-ray crystal data and the structure solution as well as the refinement are given in Table 1. A summary of selected bond lengths [Å] and angles [°] are given in Table S1 (ESI). CCDC 1989792.

2.4. Computational details

The initial theoretical structure of (*E*)-*N'*-(4-(dimethylamino)benzylidene)-5-methyl-*1H*-pyrazole-3-carbohydrazide (**3**) was that experimental determined by X-ray crystal data taken from the corresponding CIF file. The optimizations in gas phase and in aqueous solution were performed with the Revision A.02 of Gaussian09 program [67] and the hybrid B3LYP/6-311++G** method [40,41]. The cationic species of (**3**) was also optimized because it is expected in solution. The IEFPCM and universal solvation methods were employed in the optimization of (**3**) in solution because the solvent effects are considered with both models [52-54]. The Moldraw program was used to compute the volumes in both media [68]. Atomic Merz-Kollman (MK) [69] and natural population analysis (NPA) charges, molecular electrostatic potential (MEP) and stabilization energy were predicted with the version 3.1 of NBO program [70,71] while the topological properties were computed by using the AIM2000 program [72]. The mapped MEP surface of (**3**) was generating with the version 5.0 of *GaussView* program [73] while the normal internal coordinates together with the SQMFF methodology and the version 7.0 of Molvib program [55-57] were employed in the vibrational

study. To perform the assignments, only potential energy distribution (PED) contributions ≥ 10 % were considered. The predicted Raman spectrum in the gas phase in activities was corrected to intensities with the equations suggested in the literature [74]. The Ultraviolet-visible spectrum was also predicted in aqueous solution by using the Time-dependent DFT calculations (TD-DFT) [67] by using NStates=100 and the B3LYP/6-311++G** method. The predicted ^{1}H- and ^{13}C-NMR spectra in solution by using the GIAO method [75] with the hybrid B3LYP/6-311++G** method were compared with those experimental obtained in DMSO-d_6 solution. Finally, the reactivities and behaviours of (**3**) in both media were predicted with the frontier orbitals calculated with the B3LYP/6-311++G** level of theory. From the difference between both orbitals were computed the gap values and the chemical potential (μ), electronegativity (χ), global hardness (η), global softness (S), global electrophilicity index (ω) and nucleophilicity indexes (E) descriptors [36-39,42-51].

2.5. Antidiabetic activity

The α-glucosidase, β-galactosidase and α-amylase inhibition assays were conducted according to previously reported protocols [31, 76].

2.6. Antioxidant activities

The antioxidant activities of the title compound were determined *in vitro* by 2,2-diphenyl-1-picrylhydrazyl (DPPH), 2,2'-azino-bis(3-ethylbenzothiazoline-6-sulphonic acid (ABTS) and ferric reducing antioxidant power (FRAP) methods according to the procedures described in our previous work [31].

3. Results and discussion

3.1. X-ray crystal structure description

The compound **3** was analysed by single crystal X-ray diffraction. The summary of crystallographic information is listed in Table 1. The compound **3** crystalized in the monoclinic space group $P2_1/c$. The molecule is almost planar and forms dihedral angles between the central plane of the carbohydrazide moiety and the plane of the pyrazole ring (6.64^{o}) or the plane of the benzene ring (11.66^{o}). The unit cell contains four molecules. The crystal packing (Figure 1) shows that two by two molecules are arranged in parallel plans within a distance of ~10.2Å and there are no supramolecular interactions between them. Crystal packing for **3** along *a*, *b* and *c* axes are shown in Figures S1-S3.

3.2. Optimization geometry and properties in both media

Calculated total and corrected by ZPVE energies, dipole moments and volumes of (*E*)-*N'*-(4-(dimethylamino)benzylidene)-5-methyl-*1H*-pyrazole-3-carbohydrazide (**3**) as free base and cationic species in gas phase and in aqueous solution are presented in Table 2 by using the B3LYP/6-311++G** and B3LYP/6-31G* methods while the theoretical optimized structure for the free base can be seen in Figure 2 together with the atoms labelling. The cationic structure is presented in Figure S4. The phenyl ring is identified as R1 in those two species of (**3**) while R2 is designed to the pyrazole ring. The analyses of the results show a very important contraction in the volume of (**3**) as free base in aqueous solution and a strong increase in the dipole moment value is also observed with the B3LYP/6-311++G** method. On the contrary, an expansion in the volume of free base of (**3**) in aqueous solution is observed with the other method and a slight diminishing in the dipole moment value while the cationic species with the B3LYP/6-31G* method reveals a decrease or contraction of volume in aqueous solution. The expansion or contraction of volume observed for both species of (**3**) in solution can be easily attributed to the presence of group donors of H bonds, such as the O and N atoms and, to the presence of acceptors N-H groups in the structure of (**3**). Here, the formations of H bonds in solution justify the variations of those two properties in solution because (**3**) is clearly a weak base. Table S1 shows the values of Mulliken, Merz-Kollman and NPA charges, molecular electrostatic potentials (MEP) and bond orders, expressed as Wiberg indexes of free base of (**3**) in gas phase and in aqueous solution by using B3LYP/6-311++G** level of theory. In general, we observed that the MK and NPA charges present practically the same signs on the five N atoms and the only O atom but the values are different between them and different from the Mulliken charges. However, the NPA charges practically do not present changes in solution, as compared with the corresponding values in gas phase. Regarding the atomic charges in solution, it is observed that the cationic species of (**3**) could be formed by the protonation of N11 and N23 atoms but the higher Mulliken charges predict a higher value on N11 atom while the MK charges predict a most negative value on N23 (-0.493 a.u.) than the corresponding to N11 (-0.245 a.u.) indicating, this way, that the protonation could occur in the N23. Here, the calculations performed for both probable cationic species have shown all positive frequencies when the optimized cation is protonated in the N23 while two imaginary frequencies are obtained when the cation is protonated in the N11. Consequently, the cationic species of (**3**) in solution indicate the protonation of N23 atom.

Other interesting property studied here for (**3**) are the molecular electrostatic potentials (MEP) calculated from the MK charges [69] on the N and O atoms whose results are given in Table S1. Analyzing the MEP values on those atoms obtained for the free base of (**3**) by using the B3LYP/6-311++G** level of theory it is observed few changes in solution, but when the mapped MEP surface is evaluated for (**3**) in gas phase with the other basis set from Figure S5 different colorations are clearly observed on its surface. Thus, the strong red colours on the O16, N11 and N23 atoms indicate nucleophilic sites while on the H14 and H22 atoms that belong to the N13-H14 and N19-H22 bonds are observed blue colours that clearly indicate electrophilic sites. Hence, reactions with potential electrophiles or nucleophiles biological reactive take places on those two important reaction sites.

If now, the bond order (BO), expressed as Wiberg index are analyzed for (**3**) from Table S1, it is observed that N19 atom presents the higher value in both media because this atom is linked to the most labile H22 atom and, for this reason, the strong blue coloration on the mapped MEP surface it is observed on this atom. In general, the values for all atoms decrease in solution with exception of BO for the N11 and N23 atoms which increase in this medium due to the hydration with water molecules.

Taking into account the changes predicted for (**3**) in solution, corrected and uncorrected solvation energies by the total non-electrostatic terms and by zero point vibrational energy (ZPVE) of free base and cationic species of (**3**) by using the B3LYP/6-311++G** and B3LYP/6-31G* methods are compared in Table 3. Comparisons of corrected solvation energy (ΔG_c) for those two species of (**3**) with those predicted for the free base and cationic species of naloxone [77], cocaine [78] and scopolamine [79] by using the B3LYP/6-31G* method are shown in the same table because these three species show similar solvation energy values in aqueous solution although they present different biological properties. On the other hand, the structure of (**3**) has two CH_3 groups in the N33 atom, as also is observed in the structures of cocaine [78] and scopolamine [79] but, in (**3**) that N23 atom has sp^2 hybridization, different from the other compounds with sp^3 hybridization and only one CH_3 group. On the contrary, naloxone also presents the N atom in sp^3 hybridization but linked to an allyl chain and to two CH_2 of ring [77]. Structures of compared compounds can be seen in Figure S6. Probably, the sp^2 hybridization of N23 atom in (**3**) could justify the differences in the biological properties observed for this species, in relation to the other compared species [77-79]. Despite the calculations were performed with different methods, the values show that (**3**) as free base presents a higher ΔG_c (-117.85 kJ/mol by using the 6-31G* basis set and -129.50 kJ/mol by

using the other basis set) than the other ones while the cationic species evidence higher values, as expected because these species are charged and, for these reasons, they are hydrated in solution. Note that the cationic species of (3) presents a ΔG_c value between the naloxone and scopolamine species.

3.4. Geometrical parameters

The optimized geometrical parameters of (*E*)-*N'*-(4-(dimethylamino)benzylidene)-5-methyl-*1H*-pyrazole-3-carbohydrazide (**3**) as free base in gas phase and aqueous solution by using the B3LYP/6-311++G** method are presented in Table 4 together with the corresponding experimental ones determined in this work. Root-mean-square deviation (RMSD) values are also included in that table to evaluate the differences between theoretical and experimental results. Hence, good correlations are observed for bond lengths and angles with RMSD values between 0.018 and 0.012 for bond lengths and of 1.3 and 1.2 for bond angles. The higher deviations are clearly observed for dihedral angles because the C1-C12-N11-N13 dihedral angle in gas phase presents a negative value while change at positive in solution, in accordance to experimental one. On the contrary, the C12-N11-N13-C15, N13-C15-C17-N23 and C15-C17-N23-N19 dihedral angles are predicted in both media with negative signs but experimentally they have positive signs and different values. A contrary resulted is observed for the other two N13-C15-C17-C18 and O16-C15-C17-N23 dihedral angles because they are predicted in both media with positive signs and experimentally both present negative signs and different values. Evidently, the changes in the geometrical parameters of (**3**) in solution are related to its hydration and to high solvation energy observed in this medium. The good correlations evidenced in the bond lengths and angles, despite the differences observed in some dihedral angles, indicate that the optimized structures of (**3**) in both media by using the B3LYP/6-311++G** method can be used to perform the vibrational analysis and the determination of force fields in the two media.

3.5. NBO and AIM studies

The study of stability of (**3**) in both media is a very important factor taking into account that structurally this species presents acceptors and donors groups and, also reveals *in vitro* antidiabetic and antioxidant activities. Both NBO and AIM calculations are tools useful to investigate the presence of different interactions by using respectively the Second Order Perturbation Theory Analysis of Fock Matrix in NBO Basis and the topological properties according to the Bader's theory of atoms in molecules (AIM) [70-72]. In the first study the

version 3.1 of NBO program was employed [70]. Hence, main delocalization energies for the free base of (**3**) by using the B3LYP/6-311++G** method in gas phase and aqueous solution are summarized in Table S2. The evaluation of results shows that for (**3**) in gas phase are observed only four interactions: $\Delta E_{\pi\rightarrow\pi^*}$, $\Delta E_{LP\rightarrow\sigma^*}$, $\Delta E_{LP\rightarrow\pi^*}$ and $\Delta E_{\pi^*\rightarrow\pi^*}$ interactions with low energy values while in solution the $\Delta E_{\pi\rightarrow\sigma^*}$ interaction together with other two additional $\Delta E_{\sigma\rightarrow\sigma^*}$ and $\Delta E_{\sigma\rightarrow\pi^*}$ transitions with surprisingly high energy values are observed. In these two latter interactions are involved transitions of both rings and of N33 atom with both CH_3 groups. Hence, in total six interactions are observed for (**3**) in aqueous solution. Therefore, the total energy value highly favours to the free base of (**3**) in solution whose value justifies its high solvation energy value and high stability in water. Probably, this resulted indicates that the free base species of (**3**) is as a cationic species in solution because it is hydrated.

NBO analyses have shown high stability of (**3**) in solution, as compared with the values in gas phase and, for this reason, the presences of other inter or intra-molecular interactions of free base should be investigated in both media by using the topological properties, according to the Bader's theory [71]. To perform these calculations, the version 2000 of AIM program was used [72]. Hence, in Table S3 is presented the analysis of the electron density, $\rho(r)$, the Laplacian values, $\nabla^2\rho(r)$, the eigenvalues $(\lambda1, \lambda2, \lambda3)$ of the Hessian matrix and, the $|\lambda1|/\lambda3$ ratio calculated in the Bond Critical Points (BCPs) and Ring critical point (RCPs) for the free base of (*E*)-*N'*-(4-(dimethylamino)benzylidene)-5-methyl-*1H*-pyrazole-3-carbohydrazide (**3**) in gas and aqueous solution phases by using the B3LYP/6-311++G** method. These results show that in gas phase only the two expected RCP1 of ring 1 (R1) and RCP2 of ring 2 (R2) are observed while two Bond Critical Points (C4-H5···H31 and C7-H8···H35) and two new Ring critical points (RCPN1 and RCPN2) appear in solution. Obviously, those two BCPs present the characteristics of an interaction ionic or highly polar covalent where $\lambda1/\lambda3 < 1$ and $\nabla^2\rho(r) > 0$ (closed-shell interaction). In Figure 3 can be seen the molecular graphics of (**3**) in aqueous solution showing the two BCPs C4-H5···H31 and C7-H8···H35, two RCP1 and RCP2 and, the two RCPN1 and RCPN2. The presence of two BCPs in solution predict the high stability of (**3**) in this medium, as also was predicted by NBO calculations.

3.6. Vibrational study

Both B3LYP/6-31G* and B3LYP/6-311++G** methods have optimized the structures of free base and cationic species of (**3**) in gas phase and aqueous solution with C_1 symmetry and due to the presence of 37 atoms in the structure of free base 105 vibration modes are expected for

this species while for the cationic one are expected 108 vibration modes. The vibration modes of both species present activity in both spectra. The experimental FT-IR spectrum of the title compound was recorded in a solid state using reflectance (ATR) mode. A comparison of experimental ATR spectrum of free base of (**3**) in the solid phase with the corresponding predicted for free base and cationic species in gas phase by using the B3LYP/6-311++G** method can be seen in Figure 4. The group of IR bands between 2867 and 2633 cm^{-1} together with the decreasing in the intensity of IR band at 1742 cm^{-1} attributed to C=O stretching mode, predicted with high intensity by SQM calculations, could probably justify the presence of cationic species of (**3**). According Figure 4, the predicted ATR spectrum of cationic species shows higher and lower intensities of bands associated respectively to the stretching modes of N-H group of pyrazine ring and C=O bond. On the other hand, the higher number of predicted IR bands in approximately the same 4000-2000 and 2000-0 cm^{-1} regions could also support the presence of cationic species in the solid phase. In the determination of force fields for the two species of (**3**) the normal internal coordinates were employed together with the SQMFF methodology and the version 7.0 of Molvib program [55-57]. In the assignments, only potential energy distribution (PED) contributions ≥ 10 % were considered. The predicted Raman spectra for those two species in the gas phase in activities were transformed to intensities and both are observed in Figure S7. These transformations were performed with the equations suggested in the literature [74]. In Table 5 are summarized observed and calculated wavenumbers and assignments for the free base and cationic species of (**3**) in gas phase by using the B3LYP/6-311++G** method. A brief discussion by regions is presented below.

Band Assignments

4000-2000 cm^{-1} region. This region is typical of N-H, C-H and CH_3 stretching modes. Here, the free base presents two N-H stretching modes (predicted at 3494 and 3348 cm^{-1}) while for the cationic species are expected three N-H stretching modes at 3401, 3316 and 2889 cm^{-1} where this latter band is attributed to N19-H22 bond of pyrazine ring. In the cationic species, the N19-H22 stretching mode is predicted very intense in gas phase by B3LYP/6-311++G** calculations. In heterocyclic compounds, the N–H stretching vibrations appears strongly in the region 3500–3000 cm^{-1} [36,50,80]. Pillai et al. [81] have reported NH stretching bands at 3517 cm^{-1} for pyrazole and at 3388 cm^{-1} for carbohydrazide (-CONH-N=). In the present study, the FT-IR band appears at 3232 cm^{-1} is assigned to N–H stretching modes of vibrations for pyrazole and carbohydrazide, respectively. The C-H stretching vibrations of aromatic

rings give rise to bands in the region 3200–3000 cm^{-1} in aromatic compounds [38,43-48,77-80]. The C-H stretching modes for the two species are predicted by SQM calculations in approximately the same regions and, for these reasons, the ATR bands between 3141 and 2633 cm^{-1} are assigned to these vibration modes. Here, the band at 3116 cm^{-1} is assigned to C-H stretching vibrations of pyrazole ring, which is in good agreement with the values reported for pyrazole derivatives [81]. The CH stretching modes for para-substituted benzenes are found in the region 3100-3000 cm^{-1} [43-48,77-80]. The series of IR bands between 3026 and 2915 cm^{-1} were assigned as CH stretching modes of the 4-dimethylaminobenzyl ring. The C-H stretching mode of azomethine appears as a weak band at 2867 cm^{-1} in the infrared spectrum. Methyl stretching vibrations are observed in the region 2975-2765 cm^{-1} [36,43,45-47,49-51,77-80]. Note that in the cationic species the symmetric CH_3 stretching modes of three groups are predicted at 2810, 2796 and 2776 cm^{-1} while for the free base are not predicted bands in this region, for these reasons, the presence of cationic species in the solid phase could be clearly justified with the experimental IR bands at 2806, 2723 and 2633 cm^{-1}. The presence of an adjacent group such as a N or O atom can result in a significant frequency shift in the methyl (CH_3) in-phase stretch to lower frequency. Due to the absence of experimental Raman spectrum the symmetries of corresponding CH_3 stretching modes were not confirmed.

2000-1000 cm^{-1} region. In this region are expected the C=O, C=C, C-C and C-N stretching modes, deformation and rocking modes of NH, CH and CH_3 groups and, some deformations of pyrazole and 4-dimethylaminobenzyl rings can also be observed. The C=O stretching mode is usually one of the most representative in an infrared spectrum, it appears in a wavenumber region relatively free of other vibrations (1800–1600 cm^{-1}) [45-47,77-79]. This mode was assigned at 1691 cm^{-1} by Pillai et al. [81]. In our study, the SQM calculations predict that stretching mode in the free base as an intense band at 1711 cm^{-1} while in the cationic species this mode is also predicted intense at 1604 cm^{-1}. On the other hand, the C7-H8 in-plane deformation mode in free base is predicted with double intensity, as compared with the C=O vibration, according Figure 4. However, such prediction is no experimentally observed probably due to the inter-molecular hydrogen bonds between N1-H1···O1i, as determined in the experimental structure. Here, it is necessary to clarify that the theoretical calculations were performed in the gas phase where the packing forces were not considered, hence, the differences among the predicted spectra and the corresponding experimental one. Then, the C=O stretching modes for both species can be assigned to the strong IR band at 1648 cm^{-1}.

The C=C stretching of both species are predicted between 1611 and 1502 cm^{-1}, hence, these modes are assigned to group of intense IR bands between 1648 and 1522 cm^{-1}. Pillai et al. [81] have reported the stretching vibrations νC=N at 1553 cm^{-1} and νN-N at 1108 cm^{-1} in pyrazole derivative while in the carbohydrazide the C=N and C-N stretching bands are expected in the range 1672-1566 cm^{-1} and 1275 ± 55 cm^{-1}, respectively [82]. Therefore, the, intense bands observed at 1611 and 1549 cm^{-1} are assigned to C12=N11 stretching modes of free base and cationic, respectively. In the free base, the C-N stretching mode is assigned at 1549 cm^{-1} and C-N stretching mode is assigned at 1250 cm^{-1}. The N-N stretching mode has been reported at 1118 cm^{-1} by Sheeja *et al.* [82] at 1066 cm^{-1} by Govindarasu *et al.* [83] and, at 1156 cm^{-1} by Freitas *et al.* [84]. The N19-N23 and N11-N13 stretching modes in the free base and cationic species of (**3**) are assigned respectively at 1170 and 1062 cm^{-1} and, at 1182 and 1020 cm^{-1}, as predicted by calculations. In the cationic species the N11-N13 stretching mode can be also assigned to the very strong IR band at 1128 cm^{-1} because in that position this mode is observed coupled with other vibration mode.

In para substituted benzene, the C-H in-plane bending or deformations (β) vibrations are observed in the region 1400-1000 cm^{-1} and are usually of medium to weak intensity [36,49-51,77-79,81]. Here, some bands due to C–H in-plane bending vibration in both species interact somewhat with other vibrations and they can be assigned to the bands in the region between 1475 and 1136 cm^{-1}. The N13-H14 in-plane deformation corresponding to carbohydrazide group in both species is predicted at higher wavenumbers than the other N19-H22 and N23-H38 ones. Hence, the IR bands at 1549, 1408 and 1255 cm^{-1} are assigned to those vibration modes.

The deformation and rocking modes of the CH_3 groups in both species can be assigned respectively to the IR bands observed between 1461/1338 and 1158/961 cm^{-1}, as predicted by calculations and as observed in compounds with similar groups [45,47,50,78,79].

1000-10 cm^{-1} region. In this region, the C-C and C-N stretching modes, C-H and N-H out-of-plane deformations, deformations, wagging and twisting modes of C=O group, twisting CH_3 and deformations and torsions modes of both pyrazole and 4-dimethylaminobenzyl rings are expected. These vibration modes were assigned taking into account the SQM calculations performed here and by comparison with assignments for similar species [18-25,34-44]. A detail is presented in Table 5. The C=O in-plane deformation and the out-of-plane deformation are expected in the regions 625 ± 70 and 540 ± 80 cm^{-1}, respectively [81]. Here,

the IR bands observed at 904 and 742 cm^{-1} are assigned to these modes corresponding to free base while these modes for the cationic species are predicted at 667 and 362 cm^{-1}, for which, they can be assigned in this region.

The out-of-plane CH deformations are observed between 900 and 600 cm^{-1} [36,37,39,45,48-51,77-80]. Generally the CH out-of-plane deformations typical for para substituted benzenes are assigned in the 840 ± 50 cm^{-1} region [83]. In the present work, these vibration modes in the both species can be associated to the IR bands observed between 983 and 765 cm^{-1} while the corresponding N-H out-of-plane deformations are predicted and assigned to the bands observed between 734 and 501 cm^{-1}. The remaining vibration modes are assigned within the characteristic region and reported in Table 5.

3.7. Force Fields

The character of different bonds can be also descript by the harmonic force constants and, for these reasons, for free base and cationic species of (**3**) these parameters were calculated from the corresponding harmonic force fields expressed in internal coordinates. Hence, the SQMFF procedure and the Molvib program were employed [55-57]. In Table 6 those constants for both species in gas phase by using the B3LYP/6-311++G** method were compared with the reported for the free base and cationic species of naloxone and scopolamine in the same medium by using the B3LYP/6-31G* method [77,79]. Comparing first both species of (**3**), in the cationic species it is observed that due to additional N23-H38 bond the value of its force constant obviously decreases from 6.42 mdyn $Å^{-1}$ in the free base to 5.72 mdyn $Å^{-1}$ in the cationic one. Also, the $f(\nu C{=}O)$ force constant in the cationic species decreases, as compared with the corresponding to the free base. This difference in the value can be clearly attributed to the bond lengths between both involved atoms because in the free base the predicted C=O distance is 1.209 Å while in the cationic ones is 1.248 Å. Comparisons with the other two species show that the free base of (**3**) presents approximately the same value than that observed in scopolamine. On the other hand, the $f(\nu C\text{-}H)_{R1}$ force constant of 4-dimethylaminobenzyl ring in the two species of (**3**) have practically the same values than those observed for naloxone and scopolamine while the $f(\nu C\text{-}H)_{R2}$ force constants for the pyrazole ring decrease slightly in the cationic species, in relation to the free base [77,79]. The $f(\nu N\text{-}CH_3)$ force constants have practically the same values in both species of (**3**) but in naloxone and scopolamine the values change because its cationic species are formed in the N atom that contain the CH_3 groups [77,79]. Note that the $f(\nu C\text{-}N)_{Chain}$ force constant of cationic

species presents a lower value than that observed for the free base, indicating this way, that the carbohydrazide group is influenced by the N23-H38 bond. In the same way, the $f(\nu C\text{-}N)_R$, $f(\nu N\text{-}N)_R$, $f(\nu N\text{-}N)_{Chain}$ and $f(\nu C{=}C)_{R2}$ force constants change in the cationic when they are compared with the corresponding to free base. Evidently, the $f(\nu N\text{-}N)_R$ force constant (3.90 mdyn $Å^{-1}$) in the cationic species is most influenced that $f(\nu N\text{-}N)_{Chain}$ force constant of carbohydrazide group (6.73 mdyn $Å^{-1}$), as expected because the N23-H38 belong to pyrazole ring. Moreover, the cationic species generate a increase in the $f(\nu C{=}C)_{R2}$ force constant of pyrazole ring, as compared with the corresponding to $f(\nu C{=}C)_{R1}$ force constant of 4-dimethylaminobenzyl ring.

3.8. Ultaviolet-visible spectra

The electronic ultraviolet-visible spectra of free base and cationic species of (**3**) in aqueous solution were also predicted by using the B3LYP/6-311++G** method. The electronic spectra predicted for those two species can be seen in Figure S8. The predicted spectrum for the free base shows a maximum at 343.6 nm with a shoulder in c.a. 268.4 nm while for the cationic form the maximum can be observed in c.a. 225 nm. The intense observed band in the spectrum of free base and, expected for the cationic one, can be assigned to $\pi\rightarrow\pi^*$ transitions due to the presence of C=C double bonds of both pyrazole and 4-dimethylaminobenzyl rings and to carbohydrazide group and, also can be assigned to $n\rightarrow\pi^*$ transitions which are predicted for the two species by NBO calculations (Figure S9). In the UV-visible spectrum of cationic form the $\pi\rightarrow\pi^*$ and $n\rightarrow\pi^*$ transitions are predicted with low intensities as compared with the intense band attributed to $\sigma\rightarrow\sigma^*$ and $\sigma\rightarrow\pi^*$ transitions by using NBO analyses. Here, the high values of these latter two transitions predicted for the cationic species overlap to the $\pi\rightarrow\pi^*$ and $n\rightarrow\pi^*$ transitions. On the other hand, the shoulder observed in the predicted UV-Vis spectrum for the free base in aqueous solution could be attributed to the cationic form because it species is also expected in solution. These assignments for both species are in agreement with those reported for species containing similar rings [45-47,51].

3.9. NMR studies

The ^{1}H and ^{13}C NMR spectra of the title compounds were obtained by using TMS as an internal standard and DMSO-d_6 as solvent. Both ^{1}H and ^{13}C NMR spectra can be seen in Figures S10 and S11, respectively while the chemical shifts are summarized in Tables 7 and 8 compared with the corresponding theoretical ones for the free base and cationic species in

aqueous solution by using the B3LYP/6-311++G** and GIAO methods [75]. The ^{1}H NMR spectra corresponding to compound (**3**) are presented in Figure S10, respectively. The ^{1}H NMR spectra of the title molecule displayed a two singlets at δ 2.26 and 2.94 ppm due to CH_3 and $N(CH_3)_2$ protons, respectively. The chemical shifts of pyrazole proton (C4-H) appear as a singlet at δ 6.45 ppm. The chemical shifts of the phenyl protons appeared as two doublets at δ 6.72 and 7.46 ppm. The chemical shifts of the azomethine (N=CH) and amide (NHCO) protons appear as a singlet at 8.30 and 11.24 ppm, respectively. The chemical shifts of NH pyrazole proton appeared as singlet at δ 13.01 ppm. The ^{13}C NMR spectra of the title compound showed the chemical shifts of C=O are at 158.45 ppm. The signals at 148.42 ppm are clearly assigned for azomethine group (N=CH) chemical shifts. The signals at 105.11, 146.60 and 151.84 ppm are assigned for pyrazole carbons, while that the aromatic carbon chemical shifts of the compound occurred in the range of 112.26-140.36 ppm. In general, good correlations with low RMSD values are found when the theoretical chemical shifts for free base are compared with the corresponding experimental ones by using the root-mean-square deviation (RMSD) values. However, for the cationic species are observed higher RMSD values than those predicted for free base, thus, the low δ value predicted for δ of H22 (2.8 ppm) could be attributed to H bond formation in solution while the high RMSD value of the chemical shifts of C atoms in the cationic species is due to δ of C17 (108.2 ppm) probably because it atom is linked to N23 atom which could be protonated in aqueous solution.

3.10. ESI-MS study

The ESI-MS spectra show molecular ion peaks with m/z values 272.2 correspond to the molecular weight $[M+H]^+$. The m/z value 294.4 correspond to the sodiated molecular ion peak $[M+Na]^+$ (Figure S12). These values are in good agreement with the proposed composition for the title molecule ($C_{14}H_{17}N_5O$).

3.11. Hirshfeld surface analysis

The Hirshfeld surface analysis of the (E)-N'-(4-(dimethylamino)benzylidene)-5-methyl-1H-pyrazole-3-carbohydrazide **(3)** was performed with Crystal Explorer 3.1 program [85] to determine the possible molecular packing, intra and intermolecular hydrogen bond interactions in the structure. Additionally, this analysis allows the visualization of intermolecular interactions by such as red, blue and white different colours [86, 87]. As an input file in the program, Crystallographic Information File (cif*) of the compound was used. In Figure 5 was indicated d_{norm} mapped on Hirshfeld surface for visualizing the intercontacts

of the title compound and d_{norm} value was obtained as -0.2548 (red points) to 1.2144 a.u. (blue colors). As seen from the Figure 5, the dark red points near the C, O, N atoms result from C=O…H interactions with 2.273 Å and 2.782 Å and N-H…N interactions with 2.337 Å were observed and these regions have a significant role in the molecular packing.

Additionally, the two-dimensional fingerprint plots with their relative contributions or percentage contributions to the Hirshfeld surface were shown in Figure 6. The most important interactions were determined with H···H (51.2%), C···H/H···C (18%), N···H/H···N (12.4%), O···H/H···O (11%), and N···C/C···N (5.6%) contributions. Lastly, the percentage contributions of other intermolecular contacts are less than 2% in the Hirshfeld surface.

3.12. Antidiabetic activity

Inhibition of α-glucosidase and α-amylase can retard carbohydrate digestion, thus causing a reduction in the rate of glucose absorption into the blood. Therefore, inhibition of these enzyme activities in digestive organs is considered to be a therapeutic approach for managing diabetes (type 2). β-galactosidase is a tetrameric enzyme of historical and scientific importance. Moreover, the hydrolysis of lactose gives galactose and glucose. Intramolecular galactose transfer yields allolactose, the natural inducer of the lac operon. In the context, the title compound was evaluated in vitro against α-glucosidase, α- amylase and β-galactosidase. The result summarized in Table 9 and compared to the reference drug Acarbose and the phenolic compound Quercetin.

From the observed results in Table 9, the *in vitro* α-glucosidase inhibition study shows that the product **3** show a better activity for a concentration of 0.08 mM with percent inhibition of 79.83%, higher than that of the Acarbose as a reference (29%). The results of the β-galactosidase test reveal that the title compound has a good inhibitory activity with a percentage of 64.6%, comparable to that of Quercetin (68%) for a concentration of 3.30 mM. For the alpha-amylase inhibition test, the results obtained show that the compound **3** have a mean inhibitory activity (20.51%) relative to the Acarbose with a percentage of 36% for a concentration 3.53 mM.

3.13. Antioxidant activity

The antioxidant activity of the synthesized compound **3** has been systematically evaluated using three different assays at 3.70 mM. The scavenger capacity is determined by measuring the decrease in the absorption of the DPPH and ABTS radicals, and the results are expressed as Trolox equivalents (TE) (μg TE / mg of compound). Meanwhile, we have also evaluated

the ability of synthesized compounds to reduce Fe^{3+} to Fe^{2+} by using the Ferric Reducing Antioxidant Power (FRAP) test. These three assays are mainly used to measure the direct involvement of the compound in improving the primary antioxidant activity.

One of the most widely used methods for evaluating total antioxidant activity is the determination of DPPH% trapping activity by its simple, rapid, sensitive and reproducible procedure. The DPPH reagent allows us to determine the intrinsic capacity of a substance having groups (RH) such as -NH to give a hydrogen atom or electrons. In our study, the results are expressed as Trolox equivalents (ET) (µg ET / mg of compound), the tile compound **3** present a promising free DPPH scavenging capacity with 3.65 trolox equivalent (Table 10).

The ABTS method is based on the ability of hydrogen or electrondonating antioxidants to decolorize the performed radical monocation of (2,2′-azino-bis(3-ethyl-benzthiazoline-6-sulfonic acid) generated due to oxidation of ABTS with potassium persulfate. The radical scavenging abilities showed by the tested compounds towards this assay typically revealed that, the title molecule **3** exhibit moderate radical scavenging ability, expressed as trolox equivalents (µg Trolox/mg of compound) with value 5.02 trolox equivalents, respectively. Subsequently, we also evaluated the capacity of the synthesized compounds for reducing Fe^{3+} to Fe^{2+} by employing the ferric reducing antioxidant power (FRAP) test. The compound **3** displays the higher effect in reducing ferric to ferrous iron, expressed as ascorbic acid (AA) equivalents (µg AA/mg of compound) reaching more than 7.03 ascorbic acid equivalents (Table 10).

3.14. Frontier orbital and descriptors

The frontier orbitals studies of (**3**) are of great importance due to the antidiabetic and antioxidant activities that this synthesized species has revealed. Hence, the gap energies in both media were calculated for the free base from the differences between the highest occupied molecular orbital (HOMO) and the lowest unoccupied molecular orbital (LUMO) by using B3LYP/6-311++G** level of theory [42]. Then, the chemical potential (μ), electronegativity (χ), global hardness (η), global softness (S), global electrophilicity index (ω) and global nucleophilicity index (E) descriptors were also computed because these parameters are useful to predict the chemical reactivity and kinetic stability of these species [36-39,43-51]. Thus, a low gap value indicates that the species presents high chemical reactivity and low kinetic stability [42]. In **Table S4** are presented HOMO and LUMO orbitals, gap values and descriptors for free base of (**3**) in gas and aqueous solution phases by using the B3LYP/6-

311++G** method. The values for the free base of (**3**) were compared with those reported in gas phase for the same species of naloxone, cocaine and scopolamine in gas phase by using the B3LYP/6-31G* method [77-79]. Regarding the results for (**3**) in both media we observed a slight increases in the reactivity of free base of (**3**) in water and comparing with the values for the other three species, clearly, (**3**) is most reactive than naloxone, cocaine and scopolamine. The scopolamine species is the less reactive while the free base of (**3**) in aqueous solution has higher reactivity. The formation of cationic species of (**3**) in solution could justify the high reactivity due to its higher stability in solution, as suggested by NBO and AIM calculations. Probably, the higher reactivity of (**3**) and its antioxidant and antidiabetic activities can be attributed to $N(CH_3)_2$ group because both CH_3 groups are planar in (**3**) with the N33 atom in sp^2 hybridization, different from the other compared compounds. Hence, the higher reactivity of (**3**) in water is in agreement with the higher solvation energy values of free base and cationic species in solution. In relation, to the descriptors it is observed that both global electrophilicity (ω) and global nucleophilicity (E) indexes present higher and lower values, respectively in (**3**), as compared with the naxolone, cocaine and scopolamine [77-79]. These differences probably could be related to the dispositions planar of two CH_3 groups in (**3**) while in those three alkaloids are no planar.

3.15. Molecular docking

The docking computations are very important techniques in structure-based drug design and this method can estimate the binding-conformation mode within the target protein [88, 89]. In this section, firstly having medical and pharmacological importance (E)-N'-(4-(dimethylamino)benzylidene)-5-methyl-1H-pyrazole-3-carbohydrazide **(3)** molecule was optimized with B3LYP/6-311++G(d,p) method/basis set and was recorded as Protein Data Bank (PDB) format. In second step, the target proteins PDB:3A4A (α-Glucosidase) and peroxiredoxin 5-PDB:1HD2 (antioxidant) were identified with the help of literature and experimental activity study and they were obtained from the Protein Data Bank [90]. Additionally in the proteins water molecules and co-factors were cleaned and recorded PDB format. Here the PDBQT formats of ligand and two proteins were prepared with Discover Studio Visualizer 4.0 (DSV 4.0) software [91]. The AutoDock Vina program [92] was used for molecular docking calculations. The docking results obtained during this research were evaluated and were described as follows:

In the first instance, the active sites of α-Glucosidase protein-PDB:3A4A were determined as ARG442, ASP352, HIS351, GLU277, VAL216, ASP215, ARG213, PHE178, PHE159, HIS112, TYR72, ASP69, ASP38, TRP36, ASP34, ASN32 and ASP30 and according to these active residues the grid boxes were determined as centre_x=33.212, centre_y=-9.817, centre_z=22.508, size_x=88, size_y=46, size_z=50, spacing=0.375. The obtained docking results for (**3)**-PDB: 3A4A were given in Table 11 and Figure 7. From the experimental activity and theoretical docking results, the best results were observed in the interaction between (E)-N'-(4-(dimethylamino)benzylidene)-5-methyl-1H-pyrazole-3-carbohydrazide **(3)** molecule and α-Glucosidase protein-PDB: 3A4A. According to the theoretical affinity binding energies, the best binding was determined with -7.9 (kcal/mol) energy and active two hydrogen bonding. These two active hydrogen bondings were seen between ASP215 and H3 atom with 2.03 Å bond distance, between ARG442 and O1 atom with 3.11 Å bond distance. Additionally van der Waals, attractive charge, carbon-hydrogen bond, π-cation, π-anion, π- π-T shaped and π-alkyl interactions were determined from the Figure 7.

In the second instance, the active sites of antioxidant peroxiredoxin 5 protein PDB:1HD2 were determined as LEU149, THR147, GLN133, ARG127, SER118, SER115, ASP113, LYS93, GLU91, ALA90, GLN68, GLY66, ALA64, LYS63, CYS47, GLY46, PRO45, THR44, PRO40 and according to these active residues the grid boxes were determined as centre_x=10.129, centre_y=38.905, centre_z=22.741, size_x=80, size_y=82, size_z=112, spacing=0.375. Similarly, the obtained docking results for (**3)**-PDB: 1HD2 were presented in Table 11 and Figure 8. According to the affinity binding energies, the best binding was determined with -6.2 (kcal/mol) energy and 1 active and 1 non-active hydrogen bondings.

The active hydrogen bonding was observed between GLN68 and H3 atom with 2.07 Å bond distance, and non-active hydrogen bonding was observed between GLN92 and N7 atom with 3.11 Å bond distance. Additionally, van der Waals, carbon-hydrogen bond, π-cation and π-anion, interactions were also determined from the Figure 8.

Finally, the inhibition constants for (**3)** and PDB:3A4A and (**3)**-PDB: 1HD2 interactions were calculated as 1.61904 μM and 28.5343 μM, respectively by using $Ki=\exp(\Delta G/RT)$ equation, where, ΔG, R and T are the docking binding energy, gas constant (1.9872036×10^{-3} kcal/mol) and room temperature (298.15 K), respectively. From the molecular docking results of in silico antidiabetic and antioxidant, it is concluded that (E)-N'-(4-

(dimethylamino)benzylidene)-5-methyl-1H-pyrazole-3-carbohydrazide **(3)** molecule can be designed as potential antidiabetic agent .

4. Conclusions

Synthesis, crystal structure data, antioxidant and antidiabetic activities of (*E*)-*N'*-(4-(dimethylamino)benzylidene)-5-methyl-*1H*-pyrazole-3-carbohydrazide (**3**) are reported. The compound was experimentally characterized by using FT-IR, NMR, ESI-MS and single crystal X-ray diffraction (XRD). The molecular structures of free base and cationic species of (**3**) were determined theoretically in gas phase and aqueous solution by using B3LYP/6-31G* and B3LYP/6-311++G** methods. High solvation energy values are observed for both species of (**3**) in aqueous solution while the NBO and AIM studies support the higher stability of the cationic species in solution. The high energy values $\Delta E_{\sigma\rightarrow\sigma^*}$ and $\Delta E_{\sigma\rightarrow\pi^*}$ interactions that involve transitions of both rings and of N33 atom with both CH_3 groups, due to the planarity of both CH_3 groups linked to N atom, could support the high reactivities of its free base and cationic species, as compared with naloxone, cocaine and scopolamine. The harmonic force fields for both species were reported together with the complete vibrational assignments of 105 and 108 vibration modes expected respectively for free base and cationic species of (**3**). The harmonic force constants of free base and cationic species of (**3**) were also reported together with the Raman spectra for the two species and their electronic spectra in aqueous solution. In addition, the frontier orbitals studies have evidenced high reactivity of both species of (**3**) which justify its significant antioxidant activity, whilst showed the best activity against α-glucosidase higher than that acarbose, and showed activity against α-amylase similar to Quercetin. Finally, The molecular docking studies of the title compound revealed that it may exhibit anti-diabetic activity via inhibition of α-glucosidase PDB:3A4A enzyme.

Conflicts of interest

All authors declare that there are no conflicts of interest.

Acknowledgments

This work was supported by the WBI-COP22 Morocco project and UM5R as well as grants from CIUNT Project Nº 26/D608 (Consejo de Investigaciones, Universidad Nacional de Tucumán). The authors would like to thank Prof. Tom Sundius for his permission to use MOLVIB.

Supporting Information Available: Tables S1-S5 and **Figures S1-S12**.

References

[1] S. Rollas, S. G. Küçükgüzel. Biological activities of hydrazone derivatives. Molecules 12 (2007) 1910-1939.

[2] E. Hernández-Vázquez, S. Salgado-Barrera, J. J. Ramírez-Espinosa, S. Estrada-Soto, F. Hernández-Luis. Synthesis and molecular docking of N′-arylidene-5-(4-chlorophenyl)-1-(3,4-dichlorophenyl)-4-methyl-1H-pyrazole-3-carbohydrazides as novel hypoglycemic and antioxidant dual agents. Bioorg. Med. Chem. 24 (2016) 2298-2306.

[3] L.R.S. Dias, R.R.S. Salvador. Pyrazole Carbohydrazide Derivatives of Pharmaceutical Interest. Pharmaceuticals. 5 (2012) 317-324.

[4] D.d.C. Malvar, R. T. Ferreira, R.A. de Castro, L. L. de Castro, A.C.C. Freitas, E.A. Costa, I.F. Florentino, J.C. M. Mafra, G.E.P. de Souza, F.A. Vanderlinde, Antinociceptive, anti-inflammatory and antipyretic effects of 1.5-diphenyl-1H-Pyrazole-3-carbohydrazide, a new heterocyclic pyrazole derivative. Life Sci. 95 (2014) 81-88.

[5] F. Kratz, U. Beyer, T. Roth, N. Tarasova, P. Collery, F. Lechenault, Falken, U. Transferrin conjugates of doxorubicin: synthesis, characterization, cellular uptake, and in vitro efficacy. J. Pharm. Sci. 87 (1998) 338-346.

[6] P.V. Bernhardt, P. Chin, P.C. Sharpe, J.Y.C. Wang, D.R. Richardson. Novel diaroylhydrazine ligands as iron chelators: coordination chemistry and biological activity. J. Biol. Inorg. Chem. 10 (2005) 761-777.

[7] T.B. Chaston, D.R. Richardson. Iron chelators for the treatment of iron overload disease: relationship between structure, redox activity, and toxicity. Am. J. Hematol. 73 (2003) 200-210.

[8] M. Taha, S. Sultan, M. Azlan, S. A. A. Shah, W. Jamil, S. K. Yeap, S. Imran, M. N. Akhtar, S. Zareen, N. H. Ismail, M. Ali. Synthesis of a series of new 6-nitrobenzofuran-2-carbohydrazide derivatives with cytotoxic and antioxidant activity. New. Horiz. Transl. Med. 4 (2017) 23-30.

[9] P. B. Miniyar, S. N. Mokale, S. J. Makhija. Design and synthesis of 5-methylpyrazine-2-carbohydrazide derivatives: A new anti-tubercular scaffold. Arab J. Chem. 10 (2017) 41-46.

[10] I. Khan, M. A. Tantray, H. Hamid, M. S. Alam, A. Kalam, A. Dhulap. Synthesis of benzimidazole based thiadiazole and carbohydrazide conjugates as glycogen synthase

kinase-3β inhibitors with anti-depressant activity. Bioorg. Med. Chem. Lett. 26 (2016) 4020-4024.

[11] K. Karrouchi, E. Yousfi, N. Sebbar, Y. Ramli, J. Taoufik, Y. Ouzidan, M. Ansar, Y. Mabkhot, H. Ghabbour, S. Radi. New Pyrazole-Hydrazone Derivatives: X-ray Analysis, Molecular Structure Investigation via Density Functional Theory (DFT) and Their High In-Situ Catecholase Activity. Inter. J. Mol. Sci. 18 (2017) 2215.

[12] G.S. Hassan, S.M. Abou-Seri, G. Kamel, M.M. Ali, Celecoxib analogs bearing benzofuran moiety as cyclooxygenase-2 inhibitors: design, synthesis and evaluation as potential anti-inflammatory agents. Eur. J. Med. Chem. 76 (2014) 482-493.

[13] E. R. Baizman, A. M. Ezrin, R. A. Ferrari, D. Luttinger. Pharmacologic profile of fezolamine fumarate: a nontricyclic antidepressant in animal models. J. Pharmacol. Exp. Ther. 243 (1987) 40-54.

[14] G. Friedrich, T. Rose, K. Rissler. Determination of lonazolac and its hydroxy and O-sulfated metabolites by on-line sample preparation liquid chromatography with fluorescence detection. J. Chromatogr. B. 766 (2002) 295-305.

[15] C. Hampp, A. G. Hartzema, T. L. Kauf. Cost-utility analysis of rimonabant in the treatment of obesity. Value in Health. 11 (2008) 389-399.

[16] J. García-Lozano, J. Server-Carrió, E. Escrivà, J.-V. Folgado, C. Molla, L. Lezama. X-ray crystal structure and electronic properties of chlorobis (mepirizole) copper (II) tetrafluoroborate (mepirizole= 4-methoxy-2-(5-methoxy-3-methyl-1H-pyrazol-1-yl)-6-methylpyrimidine). Polyhedron. 16 (1997) 939-944.

[17] B. van Veggel, A. J. de Langen, S. Hashemi, K. Monkhorst, E. H. Rosenberg, D. A. Heideman, E. F. Smit. Crizotinib treatment for patients with EGFR mutation positive NSCLC that acquire cMET amplification after EGFR TKI therapy results in short-lived and heterogeneous responses. Lung Cancer. 124 (2018) 130-134.

[18] T. P. Selby, G. P. Lahm, T. M. Stevenson, K. A. Hughes, D. Cordova, I. B. Annan, T. F. Pahutski. Discovery of cyantraniliprole, a potent and selective anthranilic diamide ryanodine receptor activator with cross-spectrum insecticidal activity. Bioorg. Med. Chem. Lett. 23 (2013) 6341-6345.

[19] G. A. Herron, J. Rophail. Tebufenpyrad (Pyranica®) resistance detected in two-spotted spider mite Tetranychus urticae Koch (Acari: Tetranychidae) from apples in Western Australia. Exp. Appl. Acarol. 22 (1998) 633-641.

[20] H. Nagahori, H. Yoshino, Y. Tomigahara, N. Isobe, H. Kaneko, I. Nakatsuka. Metabolism of furametpyr. 1. identification of metabolites and in vitro biotransformation in rats and humans. J. Agric. Food Chem. 48 (2000) 5754-5759.

[21] K. Karrouchi, S. Radi, Y. Ramli, J. Taoufik, Y. Mabkhot, F. Al-aizari, M. Ansar. Synthesis and Pharmacological Activities of Pyrazole Derivatives: A Review. Molecules. 23 (2018) 134.

[22] L. W. Mohamed, M. A. Shaaban, A. F. Zaher, S. M. Alhamaky, A. M. Elsahar. Synthesis of new pyrazoles and pyrozolo [3, 4-b] pyridines as anti-inflammatory agents by inhibition of COX-2 enzyme. Bioorg. Chem. 83 (2019) 47-54.

[23] M. Wang, S. Xu, H. Lei, C. Wang, Z. Xiao, S. Jia, W. Zhu. Design, synthesis and antitumor activity of Novel Sorafenib derivatives bearing pyrazole scaffold. Bioorg. Med. Chem. 25 (2017) 5754-5763.

[24] K. Karrouchi, S. Fettach, S. Radi, J. Taoufik, Y. N. Mabkhot, S. Alterary, M. Ansar, Synthesis, Characterization, Free-radical Scavenging Capacity and Antioxidant Activity of Novel Series of Hydrazone, 1, 3, 4-oxadiazole and 1, 2, 4-triazole Derived from 3, 5-dimethyl-1H-pyrazole. Lett. Drug. Des. Discov. 16 (2019) 712-720.

[25] B. Mathew, J. Suresh, S. Anbazhagan. Synthesis, in silico preclinical evaluation, antidepressant potential of 5-substituted phenyl-3-(thiophen-2-yl)-4, 5-dihydro-1h-pyrazole-1-carboxamides. Biomed. Aging. Pathol. 4 (2014) 327-333.

[26] H. Jia, F. Bai, N. Liu, X. Liang, P. Zhan, C. Ma, X. Jiang, X. Liu. Design, synthesis and evaluation of pyrazole derivatives as non-nucleoside hepatitis B virus inhibitors. Eur. J. Med. Chem. 123 (2016) 202-210.

[27] K. Karrouchi, L. Chemlal, J. Taoufik, Y. Cherrah, S. Radi, M. E. A. Faouzi, M. Ansar. Synthesis, antioxidant and analgesic activities of Schiff bases of 4-amino-1,2,4-triazole derivatives containing a pyrazole moiety. Ann. Pharm. Fr. 74 (2016) 431-438.

[28] M. Fujinaga, T. Yamasaki, N. Nengaki, M. Ogawa, K. Kumata, Y. Shimoda, J. Yui, L. Xie, Y. Zhang, K. Kawamura, M.-R. Zhang. Radiosynthesis and evaluation of 5-methyl-N-(4-[11C]methylpyrimidin-2-yl)-4-(1H-pyrazol-4-yl)thiazol-2-amine ([11C]ADX88178) as a novel radioligand for imaging of metabotropic glutamate receptor subtype 4 (mGluR4). Bioorg. Med. Chem. Lett. 26 (2016) 370-374.

[29] M. Khoobi, F. Ghanoni, H. Nadri, A. Moradi, M. P. Hamedani, F. H. Moghadam, S. Emami, M. Vosooghi, R. Zadmard, A. Foroumadi. New tetracyclic tacrine analogs containing pyrano [2, 3-c] pyrazole: efficient synthesis, biological assessment and docking simulation study. Eur. J. Med. Chem. 89 (2015) 296-303.

[30] S. Mert, Z. Alım, M. M. İşgör, Ş. Beydemir, R. Kasımoğulları. The synthesis of novel pyrazole-3,4-dicarboxamides bearing 5-amino-1,3,4-thiadiazole-2-sulfonamide moiety with effective inhibitory activity against the isoforms of human cytosolic carbonic anhydrase I and II. Bioorg. Chem. 68 (2016) 64-71.

[31] R. R. Pillai, K. Karrouchi, S. Fettach, S. Armaković, S. J. Armaković, Y. Brik, J. Taoufik, S. Radi, M. E. A. Faouzi, M. Ansar. Synthesis, spectroscopic characterization, reactive properties by DFT calculations, molecular dynamics simulations and biological evaluation of Schiff bases tethered 1, 2, 4-triazole and pyrazole rings. J. Mol. Struct. 1177 (2019) 47-54.

[32] Z. Xu, C. Gao, Q.-C. Ren, X.-F. Song, L.-S. Feng, Z.-S. Lv. Recent advances of pyrazole-containing derivatives as anti-tubercular agents. Eur. J. Med. Chem. 139 (2017) 429-440.

[33] K. Figarella, S. Marsiccobetre, I. Galindo-Castro, N. Urdaneta, J. Herrera, N. Canudas, E. Galarraga. Antileishmanial and antitrypanosomal activity of synthesized hydrazones, pyrazoles, pyrazolo [1, 5-a]-pyrimidines and pyrazolo [3, 4-b]-pyridine. Curr. Bioact. Compd (2017) 13.

[34] R. Yang, T. Xu, J. Fan, Q. Zhang, M. Ding, M. Huang, L. Deng, Y. Lu, Y. Guo. Natural products-based pesticides: Design, synthesis and pesticidal activities of novel fraxinellone derivatives containing N-phenylpyrazole moiety. Ind. Crop. Prod. 117 (2018) 50-57.

[35] J.-J. Shi, G.-H. Ren, N.-J. Wu, J.-Q. Weng, T.-M. Xu, X.-H. Liu, C.-X. Tan. Design, synthesis and insecticidal activities of novel anthranilic diamides containing polyfluoroalkyl pyrazole moiety. Chinese. Chem. Lett. 28 (2017) 1727-1730.

[36] J. Kausteklis, V. Aleksa, M.A. Iramain, S.A. Brandán, Cation-anion interactions in 1-buthyl-3-methyl imidazolium nitrate ionic liquid and their effect on their structural and vibrational properties, J. Mol. Struct. 1164 (2018) 1-14.

[37] O. Noureddine, S. Gatfaoui, S.A. Brandán, H. Marouani, N. Issaoui, Structural, docking and spectroscopic studies of a new piperazine derivative, 1-Phenylpiperazine-1,4-diium-bis (hydrogen sulfate), J Mol. Struct. 1202 (2020) 127351.

[38] S. Gatfaoui, N. Issaoui, S.A. Brandán, T. Roisnel, H. Marouani, Synthesis and characterization of p-xylylenediaminiumbis(nitrate). Effects of the coordination modes of nitrate groups on their structural and vibrational properties, J. Mol. Struct. 1151 (2018) 152-168.

[39] O. Noureddine, S. Gatfaoui, S.A. Brandan, A. Sagaama, H. Marouani, N. Issaoui, Experimental and DFT studies on the molecular structure, spectroscopic properties, and molecular docking of 4-phenylpiperazine-1-ium dihydrogen phosphate, J Mol. Struct. 1207 (2020) 127762.

[40] C. Lee, W. Yang, R.G. Parr. Development of the Colle-Salvetti correlation-energy formula into a functional of the electron density. Phys. Rev., B37, (1988) 785-789.

[41] A.D. Becke, Density-functional exchange-energy approximation with correct asymptotic behavior. Phys. Rev. 1988, *A38*, 3098-3100.

[42] R.G. Paar, R.G. Pearson. Absolute hardness: companion parameter to absolute electronegativity. J. Am. Chem. Soc. 105 (1983) 7512-7516,

[43] M. Minteguiaga, E. Dellacassa, M.A. Iramain, C.A.N. Catalán, S.A. Brandán. Synthesis, spectroscopic characterization and structural study of 2-isopropenyl-3-methylphenol, carquejiphenol, a carquejol derivative with potential medicinal use. J Mol. Struct. 1165, (2018) 332-343.

[44] C. Ben M'leh, S.A. Brandán, N. Issaoui, T. Roisnel, H. Marouani. Synthesis, molecular structure, vibrational and theoretical studies of a new non-centrosymmetric organic sulphate with promising NLO properties, J Mol. Struct. 1171 (2018) 771-785.

[45] M. Minteguiaga, E. Dellacassa, M.A. Iramain, C.A.N. Catalán, S.A. Brandán, A structural and spectroscopic study on carquejol, a relevant constituent of the medicinal plant Baccharis trimera (Less.) DC. (Asteraceae), J Mol. Struct. 1150 (2017) 8-20.

[46] M. Minteguiaga, E. Dellacassa, M.A. Iramain, C.A.N. Catalán, S.A. Brandán, FT-IR, FT-Raman, UV-Vis, NMR and structural studies of Carquejyl Acetate, a component of the essential oil from *Baccharis trimera* (Less.) DC. (Asteraceae). J Mol. Struct. 1177 (2019) 499-510,

[47] J. Ruiz Hidalgo, A. Neske, , M.A Iramain. P.E. Alvarez, P. Leyton Bongiorno, S.A. Brandán, FT-IR, FT-Raman and UV-visible spectra of motrilin acetogenin isolated from *Annona cherimolia*, J Mol. Struct. 1196 (2019) 508-517.

[48] S. Trabelsi, N. Issaoui, S.A. Brandán, F. Bardak, T. Roisnel, A. Atac, H. Marouani. Synthesis and physic-chemical properties of a novel chromate compound with potential biological applications, bis(2-phenylethylammonium) chromate(VI), *J Mol. Struct.* 1185 (2019) 168-182.

[49] M.A. Iramain, M.V. Castillo, L. Davies, E. María, M.E. Manzur, S.A. Brandán. Structural and SQMFF study of potent insecticide 4,4-DDT combining the FT-IR and FT-Raman spectra with DFT calculations. J. Mol. Struct. 1199 (2020) 126964.

[50] J. Kausteklis, V. Aleksa, M.A. Iramain, S.A. Brandán. DFT study and vibrational assignment of 1-Butyl-3-methylimidazolium trifluoromethanesulfonate ionic liquid by using the FT-Raman spectrum. J. Mol. Struct. 1175 (2019) 663-676.

[51] M.A. Iramain, L. Davies, S.A. Brandán. Structural and spectroscopic differences among the Potassium 5-hydroxypentanoyltrifluoroborate salt and the furoyl and isonicotinoyl salts. J Mol. Struct. *1176* (2019) 718-728,

[52] S. Miertus, E. Scrocco, J. Tomasi. Electrostatic interaction of a solute with a continuum. Chem**.** Phys**.** 55 (1981) 11**7–**129.

[53] J. Tomasi, J. Persico. Molecular Interactions in Solution: An Overview of Methods Based on Continous Distributions of the Solvent. Chem. Rev. 94 (1994) 2027-2094.

[54] A.V. Marenich, C.J. Cramer, D.G. Truhlar. Universal solvation model based on solute electron density and a continuum model of the solvent defined by the bulk dielectric constant and atomic surface tensions, J. Phys. Chem. B113 (2009) 6378-6396.

[55] P. Pulay, G. Fogarasi, G. Pongor, J.E. Boggs, A. Vargha. Combination of theoretical ab initio and experimental information to obtain reliable harmonic force constants. Scaled quantum mechanical (QM) force fields for glyoxal, acrolein, butadiene, formaldehyde, and ethylene. J. Am. Chem. Soc. 105 (1983) 7073.

[56] G. Rauhut, P. Pulay. Transferable Scaling Factors for Density Functional Derived Vibrational Force Fields. J. Phys. Chem. 99 (1995) 3093-3100.

[57] T. Sundius. Scaling of ab-initio force fields by MOLVIB. Vib. Spectrosc. 29 (2002) 89-95.

[58] K. Karrouchi, M. Ansar, S. Radi, M. Saadi, L. El Ammari. Crystal structure of N′-diphenylmethylidene-5-methyl-1H-pyrazole-3-carbohydrazide. Acta Cryst E. 71 (2015) o890-o891.

[59] K. Karrouchi, S. Radi, J. Taoufik, H. A. Ghabbour, Y. N. Mabkhot. Crystal structure of N′-(4-(dimethylamino) benzylidene)-5-phenyl-1H-pyrazole-3-carbohydrazide, C19H19N5O. Z. Kristallogr. NCS. 231 (2016) 883-886.

[60] K. Karrouchi, S. Radi, J. Taoufik, H. A. Ghabbour, Y. N. Mabkhot. Crystal structure of N′-(4-methoxybenzylidene)-5-phenyl-1H-pyrazole-3-carbohydrazide, C18H16N4O2. Z. Kristallogr. NCS. 231 (2016) 835-837.

[61] K. Karrouchi, S. Radi, J. Taoufik, H. A. Ghabbour, Y. N. Mabkhot. Crystal structure of N′-(4-nitrobenzylidene)-5-phenyl-1H-pyrazole-3-carbohydrazide, C17H13N5O3. Z. Kristallogr. NCS. 231 (2016) 839-841.

[62] CrystalStructure 4.2: Crystal Structure Analysis Package, Rigaku Corporation (2000-2015). Tokyo 196-8666, Japan.

[63] O.V. Dolomanov, L.J. Bourhis, R.J. Gildea, J.A.K. Howard, H. Puschmann. OLEX2: A complete structure solution, refinement and analysis program J. Appl. Cryst. 42 (2009) 339-341.

[64] G. M. Sheldrick, Acta Crystallogr., Sect. C: Struct. Chem. 71 (2015) 3–8.

[65] C. F. Macrae, P. R. Edgington, P. McCabe, E. Pidcock, G. P. Shields, R. Taylor, M. Towler, J. Van De Streek. Mercury: visualization and analysis of crystal structures. J. Appl. Crystallogr. 39 (2006) 453–457.

[66] G. M. Sheldrick, Crystal structure refinement with SHELXL. Acta Cryst C. 71 (2015) 3-8.

[67] Gaussian 09, Revision A.02, M. J. Frisch, G. W. Trucks, H. B. Schlegel, G. E. Scuseria, M. A. Robb, J. R. Cheeseman, G. Scalmani, V. Barone, B. Mennucci, G. A. Petersson, H. Nakatsuji, M. Caricato, X. Li, H. P. Hratchian, A. F. Izmaylov, J. Bloino, G. Zheng, J. L. Sonnenberg, M. Hada, M. Ehara, K. Toyota, R. Fukuda, J. Hasegawa, M. Ishida, T. Nakajima, Y. Honda, O. Kitao, H. Nakai, T. Vreven, J. A. Montgomery, Jr., J. E. Peralta, F. Ogliaro, M. Bearpark, J. J. Heyd, E. Brothers, K. N. Kudin, V. N. Staroverov, R. Kobayashi, J. Normand, K. Raghavachari, A. Rendell, J. C. Burant, S. S. Iyengar, J. Tomasi, M. Cossi, N. Rega, J. M. Millam, M. Klene, J. E. Knox, J. B. Cross, V. Bakken, C. Adamo, J. Jaramillo, R. Gomperts, R. E. Stratmann, O. Yazyev, A. J. Austin, R. Cammi, C. Pomelli, J. W. Ochterski, R. L. Martin, K. Morokuma, V. G. Zakrzewski, G. A. Voth, P. Salvador, J. J. Dannenberg, S. Dapprich, A. D. Daniels, Ö. Farkas, J. B. Foresman, J. V. Ortiz, J. Cioslowski, and D. J. Fox, Gaussian, Inc., Wallingford CT, 2009.

[68] P. Ugliengo. MOLDRAW Program, University of Torino, Dipartimento Chimica IFM, Torino, Italy, 1998.

[69] B.H. Besler, K.M. Merz Jr, P.A. Kollman. Atomic charges derived from demiempirical methods, J. Comp. Chem. 11 (1990) 431-439.

[70] E.D. Gledening, J.K. Badenhoop, A.D. Reed, J.E. Carpenter, F.F. Weinhold, NBO 3.1; Theoretical Chemistry Institute, University of Wisconsin; Madison, WI, 1996**.**

[71] R. F.W. Bader, Atoms in Molecules. A Quantum Theory, Oxford University Press, Oxford, ISBN: 0198558651, 1990.

[72] F. Biegler-Köning, J. Schönbohm, D. Bayles, AIM2000; A Program to Analyze and Visualize Atoms in Molecules, J. Comput. Chem. 22 (2001) 545.

[73] A.B. Nielsen, A.J. Holder, *GaussView*, User´s Reference, GAUSSIAN, Inc.: Pittsburgh, PA, USA, 2000-2003.

[74] G. Keresztury, S. Holly, G. Besenyei, J. Varga, A.Y. Wang, J.R. Durig, Vibrational spectra of monothiocarbamates-II. IR and Raman spectra, vibrational assignment, conformational analysis and ab initio calculations of S-methyl-**N,N**-dimethylthiocarbamate. Spectrochim. Acta. 49A (1993) 2007-2026.

[75] R. Ditchfield, Self-consistent perturbation theory of diamagnetism. I. A gage-invariant LCAO (linear combination of atomic orbitals) method for NMR chemical shifts, Mol Phys. 27 (1974) 714–722.

[76] P. H. Li, Y. W. Lin, W. C. Lu, J. M. Hu, D. W. Huang. In vitro hypoglycemic activity of the phenolic compounds in longan fruit (Dimocarpus Longan var. Fen ke) shell against α-glucosidase and β-galactosidase. Int. J. Food Prop. 19 (2016) 1786-1797.

[77] M.J. Márquez, S.A. Brandán, DFT study of Species Derived from the Narcotic Antagonist Naloxone, Biointerface. Res. Appl. Chem. 10 (2020) 8096-8116.

[78] D. Romani, S.A. Brandán, Vibrational analyses of alkaloid cocaine as free base, cationic and hydrochloride species based on their internal coordinates and force fields. Paripex Indian J. Res. 6 (2017) 587-602.

[79] R.A. Rudyk, M.A. Checa, C.A.N. Catalán, S.A. Brandán, Structural, FT-IR, FT-Raman and ECD studies on the free base, cationic and hydrobromide species of scopolamine alkaloid, J Mol. Struct. 1180 (2019) 603-617.

[80] P. Larkin. Infrared and Raman spectroscopy: principles and spectral interpretation. Elsevier, (2017).

[81] R. R. Pillai, V. V. Menon, Y. S. Mary, S. Armaković, S. J. Armaković, C. Y. Panicker. Vibrational spectroscopic investigations, molecular dynamic simulations and molecular docking studies of N′-diphenylmethylidene-5-methyl-1H-pyrazole-3-carbohydrazide. J. Mol. Struct. 1130 (2017) 208-222.

[82] S. R. Sheeja, N. A. Mangalam, M. P. Kurup, Y. S. Mary, K. Raju, H. T. Varghese, C. Y. Panicker. Vibrational spectroscopic studies and computational study of quinoline-2-carbaldehyde benzoyl hydrazone. J. Mol. Struct. 973 (2010) 36-46.

[83] K. Govindarasu, E. Kavitha, N. Sundaraganesan, M. Suresh, M. S. A. Padusha. Synthesis, structural and spectral analysis of (E)-N′-(4-Methoxybenzylidene) pyridine-3-carbohydrazide dihydrate by density functional theory. Spectrochim. Acta A. 135 (2015) 1123-1136.

[84] L. V. de Freitas, C. C. da Silva, J. Ellena, L. A. S. Costa, N. A. Rey. Structural and vibrational study of 8-hydroxyquinoline-2-carboxaldehyde isonicotinoyl hydrazone–A potential metal–protein attenuating compound (MPAC) for the treatment of Alzheimer's disease. Spectrochim. Acta A.116 (2013) 41-48.

[85] M. Turner, J. McKinnon, S. Wolff, D. Grimwood, P. Spackman, D. Jayatilaka, M. Spackman, CrystalExplorer17; University of Western Australia: Crawley, WA, Australia, 2017, (2017).

[86] F.L. Hirshfeld, Bonded-atom fragments for describing molecular charge densities, Theoretica chimica acta, 44 (1977) 129-138.

[87] M.A. Spackman, D. Jayatilaka, Hirshfeld surface analysis, Cryst. Eng. Comm. 11 (2009) 19-32.

[88] A.C. Anderson, The process of structure-based drug design, Chem. Biol. 10 (2003) 787-797.

[89] D. Gilbert, Bioinformatics software resources, Briefings in bioinformatics, 5 (2004) 300-304.

[90] https://www.rcsb.org/, Accesion date: Feb 27, 2020 1:50 PM.

[91] http://www.3dsbiovia.com/, Accesion date: Feb 27, 2020 1:50 PM.

[92] O. Trott, A.J. Olson. AutoDock Vina: improving the speed and accuracy of docking with a new scoring function, efficient optimization, and multithreading. J. Comput. Chem. 31 (2010) 455-461.

Caption Figures

Figure 1. Single crystal X-ray molecular structure of (E)-N'-(4-(dimethylamino)benzylidene)-5-methyl-1H-pyrazole-3-carbohydrazide (**3**). Thermal ellipsoids representation with 50% probability. Olex and POV-Ray representation.

Figure 2. Theoretical molecular structure of free base of (*E*)-*N'*-(4-(dimethylamino)benzylidene)-5-methyl-*1H*-pyrazole-3-carbohydrazide (**3**), atoms labelling and identification of their rings.

Figure 3. Molecular graphic for the free base of (*E*)-*N'*-(4-(dimethylamino)benzylidene)-5-methyl-*1H*-pyrazole-3-carbohydrazide (**3**) in gas solution showing the geometry of all their bond critical points (BCPs) and ring critical points (RCPs) by using the B3LYP/6-31G* method.

Figure 4. Experimental infrared spectrum of (*E*)-*N'*-(4-(dimethylamino)benzylidene)-5-methyl-*1H*-pyrazole-3-carbohydrazide (**3**) compared with the corresponding predicted for the free base and cationic species by using B3LYP/6-311++G** level of theory.

Figure 5. dnorm mapped on Hirshfeld surface for visualizing the intercontacts of the title compound.

Figure 6. Finger plots of the title compound.

Figure 7. The molecular docking results of compound (**3**) with α-Glucosidase-3A4A protein, surfaces around ligand (a) and 2D forms (b).

Figure 8. The molecular docking results of compound (**3**) with antioxidant peroxiredoxin 5-1HD2 protein, surfaces around ligand (a) and 2D forms (b).

Table 1. Refinement parameters and crystal data for **3.**

CCDC Deposition Number	1989792
Crystal data	
Molecular Formula	$C_{12}H_{11}N_5O_3$
Molecular Weight	271.32
Crystal System, Space Group	Monoclinic, $P2_1/c$
Temperature (K)	293
a, b, c (Å)	6.6916 (7), 21.3667 (18), 10.3400 (8)
β (°)	107.684 (4)
V (Å^3)	1408.5 (2)
Z	4
Dcalc (g·cm^{-3})	1.279
Radiation type	Mo *K*α
μ (mm^{-1})	0.09
Crystal Dimension (mm)	0.40 × 0.20 × 0.10
Data collection	
Diffractometer	Rigaku R-AXIS RAPID II
No. of measured, independent and observed [$F^2 > 2.0\sigma(F^2)$] reflections	7374, 3119, 1790
R_{int}	0.062
$(\text{Sin } \theta/\lambda)_{max}$ (Å^{-1})	0.650
Refinement	
$R[F^2 > 2\sigma(F^2)]$, $wR(F^2)$, S	0.082, 0.216, 1.11
No. of reflections	3119
No. of parameters	181
H-atom treatment	H-atom parameters constrained
$\Delta\rho_{max}$, $\Delta\rho_{min}$ (e Å^{-3})	0.22, −0.29

Table 2. Calculated total and corrected by ZPVE energies (*E*), dipole moments (μ) and volumes (V) of (*E*)-*N'*-(4-(dimethylamino)benzylidene)-5-methyl-*1H*-pyrazole-3-carbohydrazide in gas and aqueous solution phases.

(*E*)-*N'*-(4-(dimethylamino)benzylidene)-5-methyl-*1H*-pyrazole-3-carbohydrazide					
B3LYP/6-311++G** Method					
Free base					
Medium	E (Hartrees)	E ZPVE(Hartrees)	μ (D)	V (Å^3)	ΔV (Å^3)
GAS	-892.9038	-892.6046	6.57	299.4	-2.6
PCM	-892.9459	-892.6450	11.89	296.8	
B3LYP/6-31G* Method					
Free base					
GAS	-892.6590	-892.3572	6.10	294.7	1.6
PCM	-892.6961	-892.3930	10.4	296.3	
Cationic					
GAS	-893.2125	-892.9039	12.89	303.3	-0.4
PCM	-893.3209	-893.0092	17.58	302.9	

Table 3. Corrected and uncorrected solvation energies by the total non-electrostatic terms and by zero point vibrational energy (ZPVE) of free base and cationic species of (*E*)-*N'*-(4-(dimethylamino)benzylidene)-5-methyl-*1H*-pyrazole-3-carbohydrazide (**3**) by using the B3LYP/6-311++G** method compared with other species with similar results.

B3LYP/6-311++G** method[a]			
Solvation energy (kJ/mol)			
Species	$\Delta G_{un}^{\#}$	ΔG_{ne}	ΔG_c
Free base			
(**3**)	-105.97	23.53	-129.50
B3LYP/6-31G* method[a]			
(**3**)	-93.90	23.95	-117.85
Naloxone[b]	-77.64	23.11	-100.75
Cocaine[c]	-42.75	28.51	-71.26
Scopolamine[d]	-56.66	18.81	-75.47
Cationic			
(**3**)	-276.20	24.12	-300.32
Naloxone[b]	-269.64	32.81	-302.45
Cocaine[d]	-216.66	38.58	-255.24
Scopolamine[e]	-279.87	30.47	-310.34

$\Delta G_{un}^{\#}$= uncorrected solvation energy; ΔG_{ne}= total non-electrostatic terms due to the cavitation, dispersion and repulsion energies; ΔG_c= corrected solvation energies. [a]This work, [b]From Ref [75], [c]From Ref [76], [d]From Ref [77]

Table 4. Comparison of calculated geometrical parameters of (*E*)-*N'*-(4-(dimethylamino)benzylidene)-5-methyl-*1H*-pyrazole-3-carbohydrazide in both media with the corresponding experimental ones.

B3LYP/6-311++G** method[a]			Experimental[a]
Parameters	Gas	PCM	
Bond lengths (Å)			
N11-C12	1.281	1.289	1.289(5)
N11-N13	1.359	1.372	1.383(4)
N13-C15	1.388	1.359	1.354(5)
C15=O16	1.209	1.238	1.235(3)
C15-C17	1.496	1.482	1.472(4)
C17-N23	1.330	1.338	1.340(3)
N19-N23	1.343	1.342	1.346(4)
N19-C20	1.362	1.360	1.357(4)
C18-C20	1.380	1.382	1.380(4)
C20-C24	1.494	1.490	1.483(5)
N33-C6	1.383	1.382	1.376(5)
N33-C29	1.454	1.461	1.450(5)
N33-C34	1.455	1.462	1.425(8)
C12-C1	1.456	1.450	1.440(5)
RMSD	**0.018**	**0.012**	
Bond angles (º)			
C1-C12-N11	122.6	123.2	123.0(3)
C12-N11-N13	117.0	115.1	114.9(2)
N11-N13-C15	121.5	121.4	120.6(2)
N13-C15-O16	124.1	123.0	122.4(3)
C17-C15-O16	123.9	122.4	122.6(3)
C15-C17-N23	119.6	118.7	120.3(3)
C15-C17-C18	129.1	130.1	128.0(2)
C17-N23-N19	104.3	104.3	103.5(3)
N23-N19-C20	114.0	113.8	113.9(2)
N19-C20-C24	122.9	122.6	122.7(3)
C4-C6-N33	121.5	121.6	121.4(3)
C7-C6-N33	121.3	121.3	121.9(4)
C6-N33-C29	119.5	118.8	120.3(4)
C6-N33-C34	119.7	118.9	122.5(3)
RMSD	**1.2**	**1.3**	
Dihedral angles (º)			
C1-C12-N11-N13	-179.3	179.8	179.3(3)
C12-N11-N13-C15	-174.4	-179.5	174.3(3)
N11-N13-C15-O16	2.1	2.2	2.1(5)
N11-N13-C15-C17	-177.1	-177.8	-177.6(2)

N13-C15-C17-N23	-149.5	-168.1	6.6(4)
N13-C15-C17-C18	31.8	12.3	-176.4(3)
O16-C15-C17-N23	31.2	11.8	-173.2(3)
C15-C17-N23-N19	-178.9	-179.8	177.9(3)
RMSD	**246.7**	**210.2**	

[a]This work, RMSD values in bold letters

Table 5. Observed and calculated wavenumbers (cm^{-1}) and assignments for the free base and cationic species of (*E*)-*N'*-(4-(dimethylamino)benzylidene)-5-methyl-*1H*-pyrazole-3-carbohydrazide (**3**) in gas phase by using the B3LYP/6-311++G** method.

Experimental[a]	B3LYP/6-311++G** Method[a]					
	FREE BASE				CATIONIC	
ATR	Calculated[b]	Intensity[c]	SQM[d]	Assignments[a]	SQM[d]	Assignments[a]
3232m	3645	111.8	3494	νN19-H22	3401	νN23-H38
3232m	3492	9.7	3348	νN13-H14	3316	νN13-H14
3141w	3245	0.7	3111	νC18-H21		
3116w	3210	12.7	3078	νC7-H8	3065	νC7-H8
3097w	3209	13.7	3076	νC4-H5	3062	νC4-H5
3079sh	3189	0.9	3057	νC9-H10	3050	νC18-H21
3064sh	3152	14.6	3022	νC2-H3	3049	νC9-H10
3026w	3129	44.3	2999	ν_aCH_3(C34)	3010	νC2-H3
2987w	3119	8.3	2990	ν_aCH_3(C24)	2974	ν_aCH_3(C34)
2983sh	3117	2.5	2988	ν_aCH_3(C29)	2966	ν_aCH_3(C29)
2971w	3073	12.8	2946	ν_aCH_3(C24)	2947	ν_aCH_3(C24)
2960w	3056	38.3	2929	ν_aCH_3(C34)	2937	ν_sCH_3(C34),ν_aCH_3(C34)
2934sh	3051	34.5	2925	ν_aCH_3(C29)	2929	ν_aCH_3(C29)
2912w	3026	37.7	2901	ν_sCH_3(C24)	2889	νN19-H22
2867w	2992	67.0	2868	νC12-H28	2866	ν_aCH_3(C24)
2853w	2980	136.7	2856	ν_sCH_3(C34)	2862	νC12-H28
2806w	2972	81.5	2849	ν_sCH_3(C29)	2810	ν_sCH_3(C34),ν_aCH_3(C34)
2723w,br					2796	ν_sCH_3(C29)
2633w,br					2776	ν_sCH_3(C24)
1742w	1774	364.8	1711	νC15=O16···H-N?		
1648s	1774	364.8	1711	νC15=O16	1604	νC15=O16,νC15-C17
1611s	1670	15.9	1611	νC12-N11		
1600vs	1647	430.3	1593	νC7-C9	1591	νC7-C9
1600vs	1609	15.7	1557	νC18-C20	1557	νC18-C20
1570m	1585	14.1	1538	νC4-C6,νC1-C2	1539	νC1-C2
1549s	1562	5.9	1529	βN13-H14	1514	νC12-N11,βN13-H14
1522vs	1540	704.2	1502	βC7-H8	1502	νC1-C12
1475m	1530	26.1	1468	δ_aCH_3(C34),δ_aCH_3(C29)	1485	βC7-H8
1468sh	1514	3.3	1452	δ_aCH_3(C29), δ_aCH_3(C34)	1461	δ_aCH_3(C34)
1444m	1506	0.2	1448	δ_aCH_3(C24)	1444	δ_aCH_3(C29)
1438sh	1495	18.8	1431	δ_aCH_3(C34), δ_aCH_3(C29)	1438	βN23-H38,δ_aCH_3(C24)
1430m	1487	15.3	1423	δ_aCH_3(C29), δ_aCH_3(C34)	1427	δ_aCH_3(C34)
	1485	26.9	1422	δ_sCH_3(C34),δ_aCH_3(C34)	1420	δ_aCH_3(C29)
	1484	7.9	1421	δ_aCH_3(C24)	1419	δ_aCH_3(C24)
1416sh	1466	27.8	1420	νC15-C17	1413	δ_sCH_3(C34)
1408m	1462	11.9	1415	νC2-C4,βC4-H5	1404	βC4-H5
1408m	1446	5.4	1394	νC17-N23,βN19-H22	1396	δ_aCH_3(C24)
1380sh	1438	5.9	1383	δ_sCH_3(C34),δ_sCH_3(C29)		
1373sh	1429	33.4	1376	νC17-C18	1376	δ_sCH_3(C29)
1359s	1415	17.5	1355	δ_sCH_3(C24)	1352	βN19-H22
1359s	1385	18.9	1349	βC12-H28	1338	δ_sCH_3(C24)
1359s	1378	317.4	1332	νC6-N33	1330	βC12-H28
1320m	1358	5.9	1320	βC9-H10,βC2-H3	1310	βC9-H10
1255s	1339	26.3	1299	νC9-C1	1297	νC6-N33
1255s	1296	12.7	1255	νC20-N19	1291	βN23-H38
1255s					1284	βN23-H38
1255s					1282	νC9-C1

1228vs	1266	40.3	1228	νC1-C12	1234	νN11-N13,βC12-H28
1213sh	1260	57.2	1217	νC6-C7	1217	βC18-H21
1182s	1228	226.6	1190	νC15-N13	1202	νC4-C6,νC6-C7
1182s	1208	100.5	1174	βC2-H3,βC9-H10	1180	νN11-N13
1182s	1191	57.9	1158	ρCH_3(C34),ρCH_3(C29)		
1170s	1171	381.8	1132	νN19-N23	1171	βC2-H3
1170s	1155	1.8	1122	βC18-H21	1147	ρCH_3(C34), ρCH_3(C29)
1136w	1147	43.9	1113	βC18-H21,νN11-N13	1136	βC18-H21,νC20-C24
1136w	1139	82.9	1109	ρ'CH_3(C29)	1119	ρ'CH_3(C34)
1097sh	1130	0.4	1100	ρ'CH_3(C34)	1109	νC2-C4
1062m	1085	2.6	1053	νN11-N13	1089	ρ'CH_3(C29)
1062m	1078	23.5	1046	ρCH_3(C34),ρCH_3(C29)	1052	γN19-H22,ρ'CH_3(C24)
1062m	1062	1.4	1035	ρ'CH_3(C24)	1040	ρCH_3(C34)
1020w	1045	5.3	1024	βR_1(A2)	1006	νN19-N23
1007w	1019	0.8	998	βR_1(A1)	995	βR_1(A1)
983w	1008	11.0	986	βR_2(A2)	989	ρ'CH_3(C24),γN19-H22
983w	989	5.8	977	γC9-H10	981	νC15-N13,νC17-N23
983w					967	ρCH_3(C24)
962w	986	1.9	961	ρCH_3(C24)	962	γC9-H10
948s	962	10.8	955	γC12-H28,γC2-H3	930	νC34-N33,νC29-N33
938sh	961	43.3	929	νC34-N33,νC29-N33	920	νC34-N33,νC29-N33
926w	934	2.7	925	γC2-H3,γC12-H28	913	γC2-H3
904s	917	61.9	902	βC15=O16	861	νC20-N19
846w					852	νN19-N23,βR_2(A2)
846w	851	17.5	832	νC9-C1,δC1C12N11	839	γC12-H28
814s	833	42.6	823	γC7-H8	812	γC7-H8
814s					807	δC15N13N11
793s	811	20.9	801	γC18-H21	796	γC18-H21
765s	808	8.8	798	γC4-H5	784	γC4-H5
742m	773	20.1	762	γC15=O16		
734sh	746	5.7	729	βR_3(A1),νC6-N33	727	γN23-H38
722sh	736	0.5	715	τR_1(A1)	715	γN23-H38,βR_3(A1)
682w	694	11.9	677	τR_1(A2)	705	τR_1(A1)
653m	675	19.4	658	νC20-C24	667	γC15=O16
639w	659	14.1	647	βR_2(A1), βR_3(A1)	649	βR_2(A1),βR_3(A1)
612m	652	1.0	641	τR_2(A2)	607	βR_1(A2), βR_2(A2)
590m	602	2.5	592	δC34N33C29,δC1C12N11	591	δC1C12N11
518s	549	37.2	542	γN19-H22	538	γN13-H14
518s	536	31.5	524	γC6-N33,γC1-C12	521	γC6-N33,γC1-C12
501m	511	6.4	506	γN13-H14, δC34N33C29	506	γN13-H14
501m	508	46.9	504	γN13-H14		
493sh	493	14.3	487	βN33-C29,βC6-N33	492	δC34N33C29
493sh					483	τR_2(A2)
468w	457	5.6	451	βN33-C29,βC6-N33	454	βN33-C29
	432	0.8	415	τR_3(A1)		
	419	0.7	411	δC34N33C29	408	τR_3(A1)
	403	0.9	385	τR_1(A1), τR_3(A1)	407	τR_3(A1)
					384	τR_1(A1),τR_3(A1)
	368	4.5	360	νC15-C17,βC15=O16	362	βC15=O16
	347	4.5	343	βC20-C24	334	τR_1(A2)
	302	3.8	296	γC20-C24,γC17-C15	318	βC20-C24
	286	0.8	281	βC6-N33	293	βC6-N33
	274	15.9	259	τR_2(A1)	251	τR_2(A1)
	234	3.5	220	τR_2(A1), τC12-C1	229	γC20-C24

212	2.6	206	βC17-C15	208	τwCH$_3$(C29), δC15N13N11
205	2.8	195	δC15N13N11,τwCH$_3$(C34)	206	τC12-C1
				194	τwCH$_3$(C24), τR$_2$(A2)
				178	τwCH$_3$(C24)
172	1.6	161	τwCH$_3$(C34), τwCH$_3$(C29)	177	τwCH$_3$(C29)
168	5.1	155	τC12-C1	162	τwCH$_3$(C34)
149	0.5	143	τR$_2$(A1), τN11-C12	159	τwCH$_3$(C34) ,τN11-N13
107	7.5	99	γN33-C29	114	τC15-C17,τR$_2$(A1)
				94	δC17C15N13,βC17-C15 βC1-C12
90	2.2	89	δC17C15N13,βC1-C12	91	τC15-C17,γC17-C15
79	4.2	73	γN33-C29,τN11-N13		
74	3.6	67	τN33-C6		
57	0.1	51	τwCH$_3$(C24)	60	γN13-H14,τN11-N13,τR$_2$(A1)
47	1.1	43	τC15-C17		
35	4.1	35	δN13N11C12 δC15N13N11, δC1C12N11	37	δN13N11C12
28	0.1	25	τN11-N13	33	τN11-N13
22	2.3	20	τN13-C15,τN11-C12	22	τN33-C6
				17	τN13-C15

Abbreviations: ν, stretching; β, deformation in the plane; γ, deformation out of plane; τ , torsion; β$_R$. deformation ring τ$_R$, torsion ring; ρ, rocking; τw, twisting; δ, deformation; a, antisymmetric; s, symmetric; (A$_1$), Ring 1; (A$_2$), Ring 2; [a]This work, [b]Intensities in KM/Mole; [c]From B3LYP/6-311++G** method, [d]From scaled quantum mechanics force field.

Table 6. Scaled internal force constants for the for the free base and cationic species of (*E*)-*N'*-(4-(dimethylamino)benzylidene)-5-methyl-*1H*-pyrazole-3-carbohydrazide (**3**) in gas phase by using the B3LYP/6-311++G** method.

Force constants	(*E*)-*N'*-(4-(dimethylamino)benzylidene)-5-methyl-*1H*-pyrazole-3-carbohydrazide[a]		Naloxone[b]		Scopolamine[c]	
	Free base	Cationic	Free base	Cationic	Free base	Cationic
$f(\nu N\text{-}H)$	6.49	5.72		5.75		6.04
$f(\nu C{=}O)$	11.69	9.15	12.47	12.76	11.65	12.08
$f(\nu C\text{-}H)_{R1}$	5.13	5.10	5.16	5.20	5.14	5.15
$f(\nu C\text{-}H)_{R2}$	5.29	5.10			4.84	4.85
$f(\nu N\text{-}CH_3)$	4.83	4.80	4.68	3.51	4.76	3.93
$f(\nu C\text{-}N)_{Chain}$	7.46	6.10				
$f(\nu C\text{-}N)_{R}$	6.74	4.32	4.91	3.86	4.27	3.20
$f(\nu N\text{-}N)_{R}$	5.85	3.90				
$f(\nu N\text{-}N)_{Chain}$	5.56	6.73				
$f(\nu C{=}C)_{R1}$	6.24	6.15	5.72	7.33		
$f(\nu C{=}C)_{R2}$	6.84	7.31				
$f(\nu CH_3)$	4.75	4.62			4.81	5.11
$f(\delta CH_3)$	0.55	0.55			0.58	0.56

Units are mdyn $Å^{-1}$ for stretching and mdyn Å rad^{-2} for angle deformations

[a]This work

Table 7. Observed and calculated ^{1}H chemical shifts (δ in ppm) for (*E*)-*N'*-(4-(dimethylamino)benzylidene)-5-methyl-*1H*-pyrazole-3-carbohydrazide (**3)** in gas phase and in aqueous solutions.

H atom	6-311++G**		Exp[a]
	Free base	Cation	
3-H	7.1	6.6	7.46
5-H	6.7	6.5	6.72
8-H	7.0	6.6	6.72
10-H	8.6	8.2	7.46
14-H	8.1	7.4	8.30
21-H	6.0	5.2	6.45
22-H	9.1	2.8	13.01
25-H	2.2	1.9	2.26
26-H	2.3	2.0	2.26
27-H	2.2	1.8	2.26
28-H	7.7	7.2	11.24
30-H	2.4	2.1	2.94
31-H	3.3	3.3	2.94
32-H	2.5	2.2	2.94
35-H	3.5	3.4	2.94
36-H	2.6	2.3	2.94
37-H	2.3	2.0	2.94
RMSD	**1.4**	**2.7**	

[a]This work GIAO/B3LYP/6-31G* Ref. to TMS

Table 8. Observed and calculated ^{13}C chemical shifts (δ in ppm) for the free base of (*E*)-*N'*-(4-(dimethylamino)benzylidene)-5-methyl-*1H*-pyrazole-3-carbohydrazide (**3**) by using the B3LYP/6-311++G** method in aqueous solution.

C atoms	6-311++G**		Exp[a]
	Free base	Cation	
1-C	128.8	138.9	122.33
2-C	136.7	129.0	128.76
4-C	114.2	115.1	112.26
6-C	158.0	149.2	151.84
7-C	117.3	116.9	112.26
9-C	133.1	128.5	128.76
12-C	148.6	123.9	146.60
15-C	160.5	155.9	158.45
17-C	152.4	108.2	148.42
18-C	104.4	108.8	105.11
20-C	142.9	126.9	140.36
24-C	10.3	13.7	10.78
29-C	39.3	40.9	40.28
34-C	39.8	40.6	40.28
RMSD	**4.0**	**13.8**	

[a]This work GIAO/B3LYP/6-31G* Ref, to TMS

Table 9. Antidiabetic activity **(3)**

Compound	% of inhibition		
	α-glucosidase	β-galactosidase	α-amylase
3	79,83	64,29	20,51
Acarbose	29	--	36
Quercetin	--	68	--

Table 10. Antioxidant activity of (**3**).

Compound	DPPH (µg ET/ mg)	ABTS (µg ET/ mg)	FRAP (µg EAA/ mg)
3	4,88 ± 0,10	5,03 ± 0,60	7,03 ± 0,50

Table 11. AutoDockVina results of the binding affinity and RMSD values of different poses in 3A4A and 1HD2 inhibitors of **(3)** compound.

Modes	**3 compound-3A4A**			**3 compound-1HD2**		
	Affinity (kcal/mol)	rmsdl.b.	rmsdu.b.	Affinity (kcal/mol)	rmsdl.b.	rmsdu.b.
1	-7.9	0.000	0.000	-6.2	0.000	0.000
2	-7.5	2.078	9.027	-5.6	21.022	21.845
3	-7.2	14.842	19.175	-5.6	20.659	23.131
4	-6.8	14.224	18.517	-5.0	7.053	9.854
5	-6.7	25.978	28.132	-4.9	15.578	18.500
6	-6.6	4.874	6.066	-4.7	6.450	8.855
7	-6.4	25.912	28.166	-4.7	19.947	20.915
8	-6.2	15.156	17.764	-4.5	12.932	13.651
9	-6.2	2.091	9.625	-4.5	24.228	25.163
10	-6.1	19.252	21.121	-4.5	24.503	26.829
Inhibition Constant: 1.61904 μM Number of Hydrogen bonding: 2 active				Inhibition Constant: 28.5343 μM Number of Hydrogen bonding: 1 active+1 non-active		

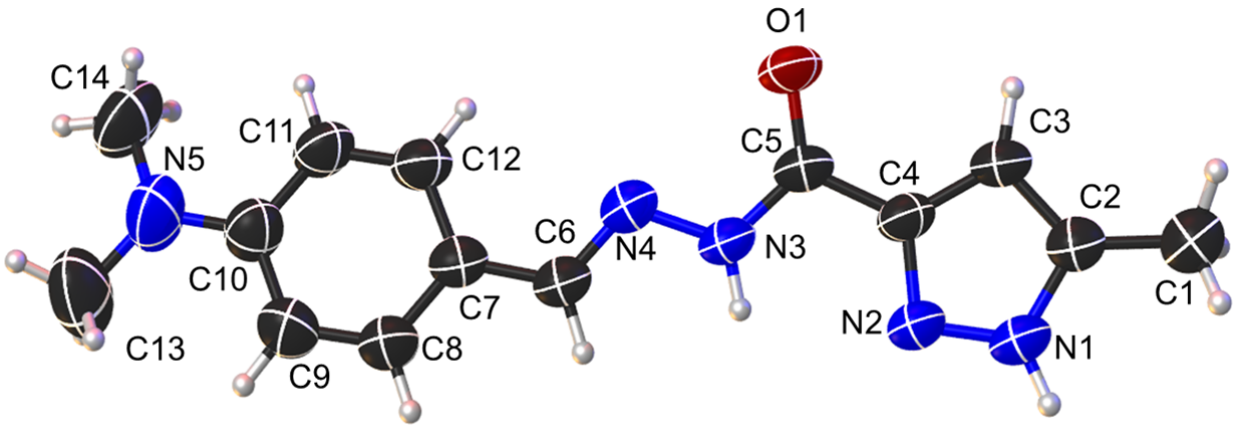

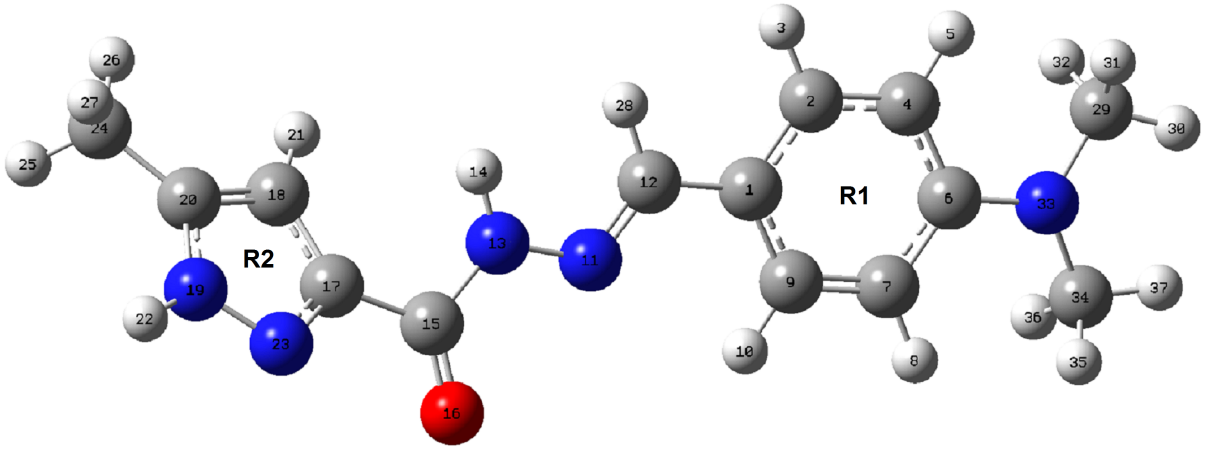

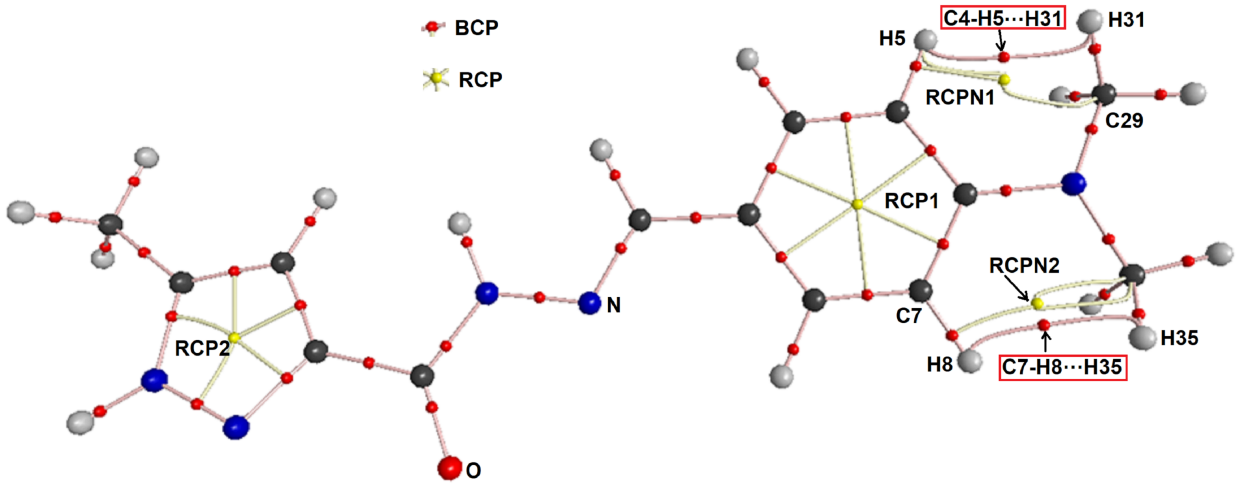

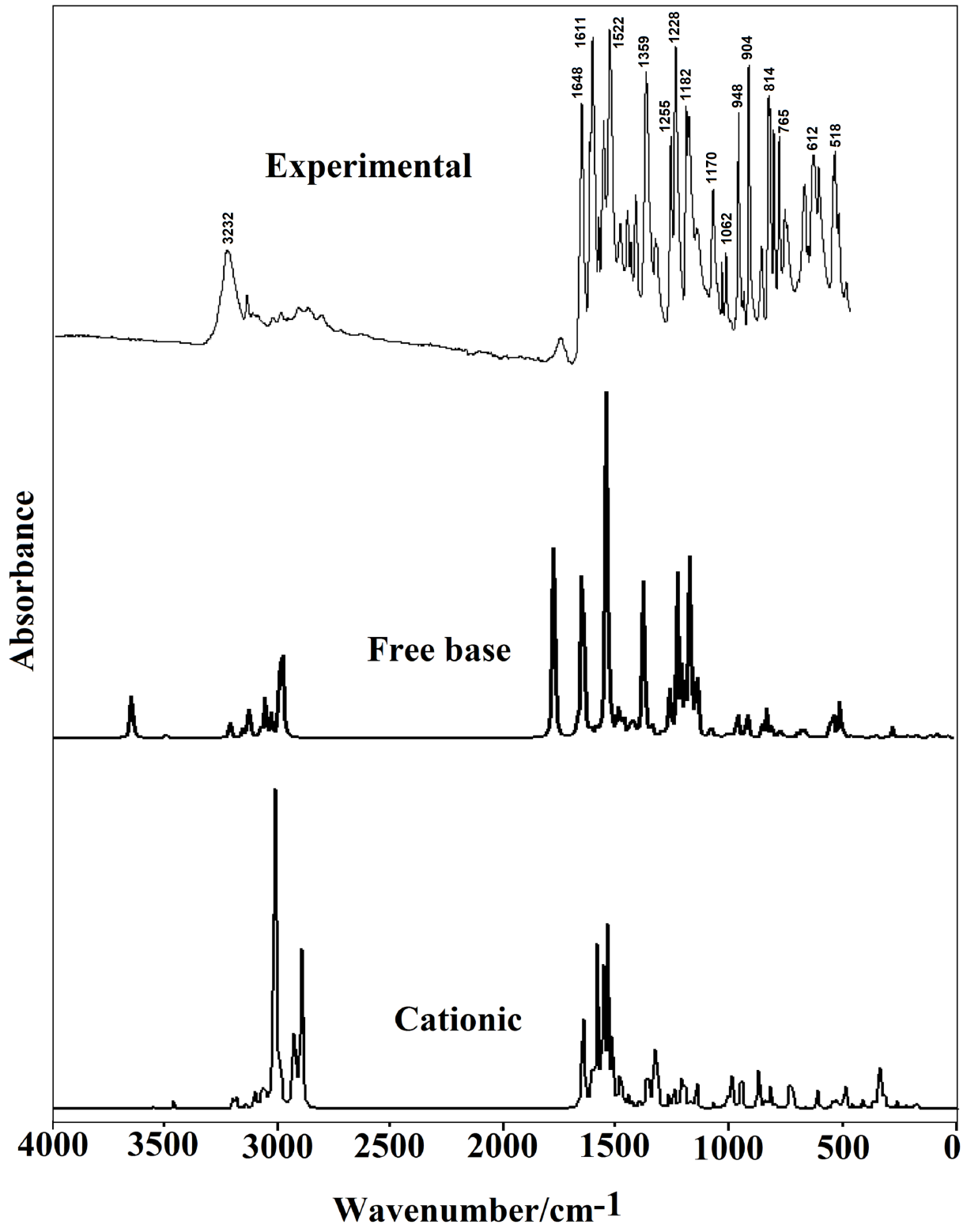
Experimental
3232
1648
1611
1522
1359
1255
1228
1182
1170
1062
948
904
814
765
612
518
Free base
Cationic
Absorbance
4000
3500
3000
2500
2000
1500
1000
500
0
Wavenumber/cm-1

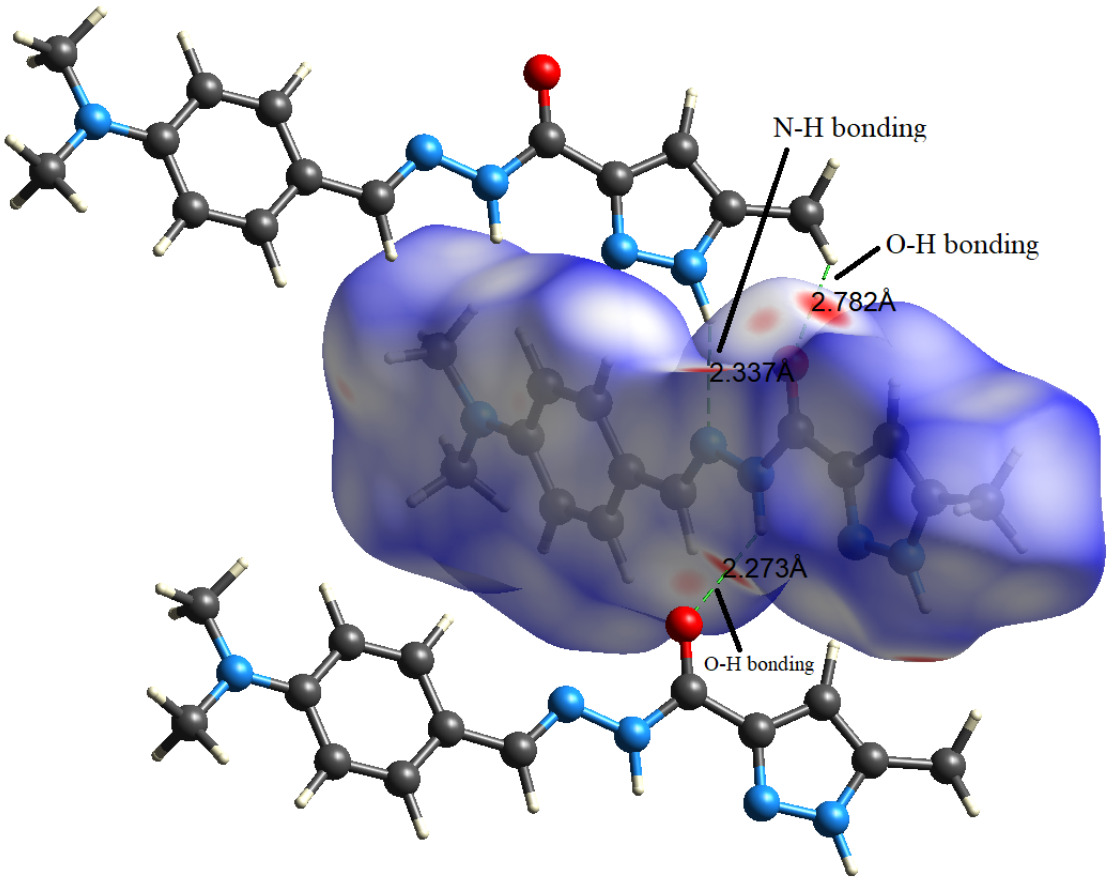

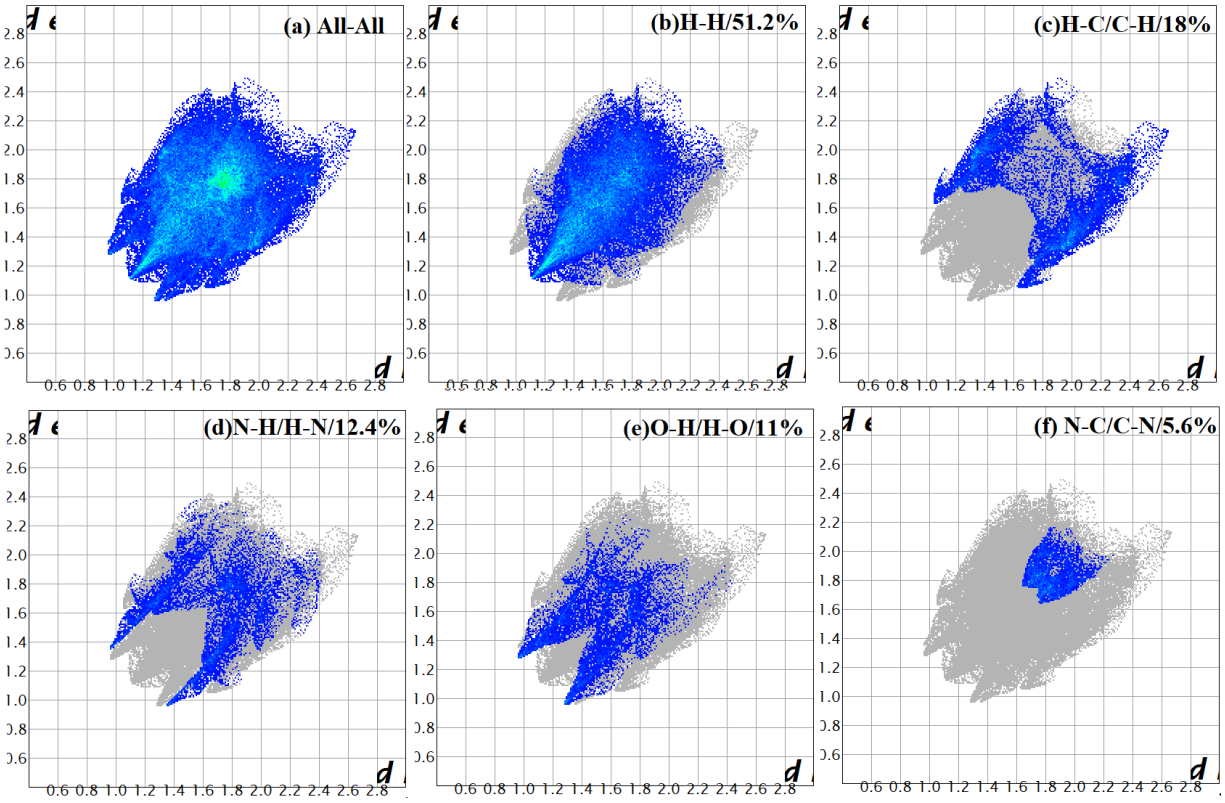

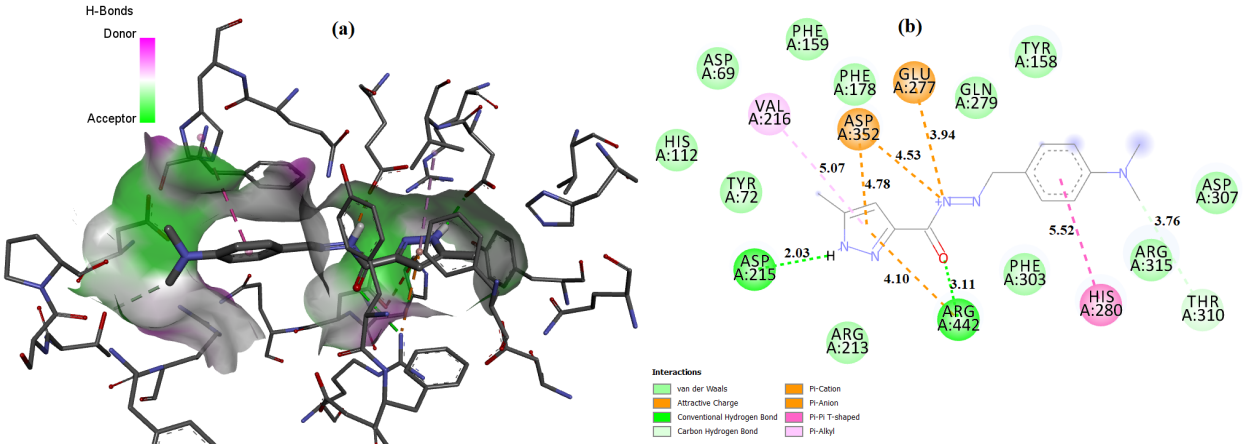

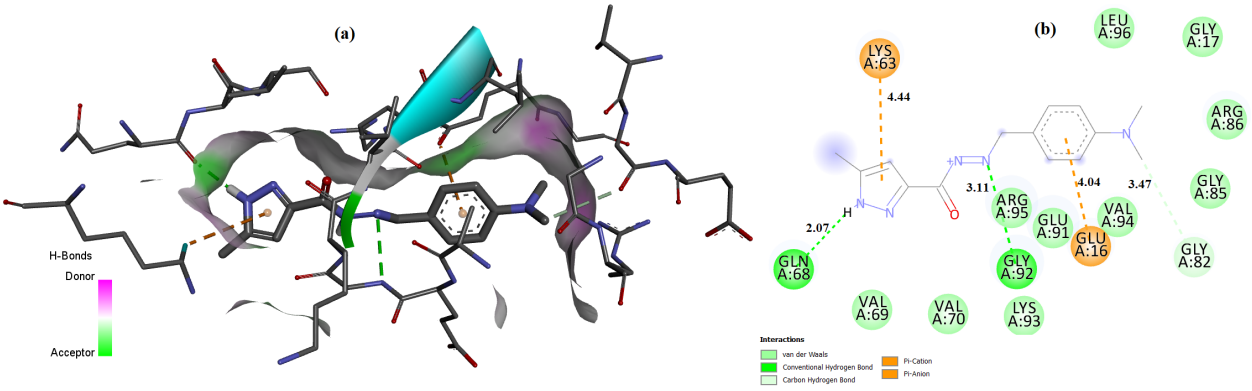

Highlights

- A new pyrazole derivative was synthesized and characterized by spectroscopic methods.
- Two species of new derivative were studied theoretically in gas phase and aqueous solution.
- High solvation energy values are observed for both species.
- NBO and AIM studies support the higher stability of the cationic species in solution.
- Complete vibrational assignments for both species and the force constants are reported.
- The anti-diabetic and antioxidant activities were tested, and Molecular docking studies were carried.

Declaration of interests

☒ The authors declare that they have no known competing financial interests or personal relationships that could have appeared to influence the work reported in this paper.

☐The authors declare the following financial interests/personal relationships which may be considered as potential competing interests: